Structure and properties of smart micro-and nanogels determined by (neutron) scattering methods

Julian Oberdisse, Thomas Hellweg

Chapter 1

Structure and properties of smart micro- and nanogels determined by (neutron) scattering methods

Julian Oberdisse[1*] and Thomas Hellweg[2*]

[1] *Soft Matter Group, Laboratoire Charles Coulomb UMR 5221 CNRS-UM cc 26, Université de Montpellier, 34095, Montpellier Cedex 05 , France*
[2] *Physical and Biophysical Chemistry, Universität Bielefeld, 33615, North-Rhine Westfalia, Bielefeld, Universitätsstr. 25, Germany*

*Corresponding Authors: Julian Oberdisse; julian.oberdisse@umontpellier.fr; Thomas Hellweg; thomas.hellweg@uni-bielefeld.de

Abstract: Meanwhile since more than three decades smart micro- and nanogels are studied and the number of publications in this area of research is steadily growing. This year to date (May 2021) already more than 400 articles were published on this topic. In the study of such colloidal gels the most important techniques besides microscopy are scattering techniques. In the present chapter an introduction to these non-destructive techniques and their application to smart micro- and nanogels will be given, and besides some fundamental works on this topic the most recent studies in this context will be discussed. We put a focus on multi-compartment and multi-

stimuli responsive microgels and review time-resolved small-angle scattering experiments. In addition one section is devoted to the study of crowded microgel systems.

Keywords: Microgel, SANS, SAXS, light scattering, stopped-flow, p-jump

1.1. Introduction

So-called smart microgels were first synthesized by Pelton and Chibante in 1986 [80]. Microgels are colloidal particles exhibiting an internal gel structure. They have diameters in the range from 100 nm up to micrometers [88, 81, 40, 73, 4, 83, 84, 54]. Below the 100 nm threshold they are called nanogels [54]. Their most striking feature is the temperature-induced reversible collapse of the polymer network which is similar to macroscopic gels [33, 111, 68, 107]. Besides a temperature-induced response, also particles with sensitivity to changes in pH, ionic strength, and other external fields can be made [109, 89, 57, 32, 60, 50] However, the internal structure of microgels seems to differ from macroscopic gels, which is due to differences in reaction kinetics of the cross-linker (in many cases *N,N'*-methylen-bis-acrylamide, BIS) and the monomer (very often *N*-isopropyl acrylamide, NIPAM).

Microgels are of steadily growing interest which is related to the plethora of potential applications ranging from drug and vaccine delivery [106, 92, 28, 12, 113, 82], over smart catalytic systems [70, 118, 11] and photonic applications [29, 108, 117] to smart surfaces for vertebrate cell manipulation [114] and responsive membranes [7, 13]. For these purposes different copolymer systems [1, 2, 65, 49] and structures exhibiting separated compartments were designed [64, 19, 62, 99, 74, 53]. Moreover, several of these systems are interesting model

colloids allowing to study particles with tunable interaction potential [103, 100]. It is even possible to generate extremely soft self-crosslinked particles which are at the edge between star polymers and well-defined colloidal particles [103]. The overall size and shape of microgels is mainly studied by static and dynamic light scattering (namely photon correlation spectroscopy (PCS)). Especially PCS is very often used to follow the temperature or pH dependent swelling and de-swelling of smart microgels. Such experiments are complemented by electron microscopy techniques and atomic force microscopy (AFM). However, these methods only hardly reveal internal structures and dynamics of microgels. Such structures are in the range from some Ångströms to some nanometers. This length-scale domain is successfully studied by small-angle scattering techniques like small-angle x-ray scattering (SAXS) and small-angle neutron scattering (SANS)[104, 105, 87], neutron and x-ray reflectometry [119] and neutron spin-echo spectroscopy [48, 91]. Recently, also x-ray PCS has been employed to follow microgel dynamics [36].

In the last 5-6 years, a lot of progress was made in the use of the above-mentioned methods. Hence, it is thus time to review some of these advances. Besides giving a comprehensive update of recent work done in this area, the present chapter also tries to provide an introduction to the basics of scattering experiments on responsive microgels. Besides PCS no inelastic experiments will be discussed. The contribution is structured as follows: in section 1.2, scattering is introduced, covering both static and dynamic light scattering, as well as small-angle scattering. In the next section 1.3, recent progress in multi-compartment and multi-stimuli responsive microgels is reviewed. Sections 1.4 and 1.5 then deal with time-resolved experiments on microgels, and a short overview of crowded microgel systems.

1.2. Scattering techniques applied to microgels

Scattering of radiation is a prominent method for investigating the micro- and nano-scopic state of matter on the scale of the wavelength of the radiation in question, and such methods have been actively used for more than a century. Since World War II, the advent of powerful sources has triggered an enormous increase in such applications. Light, X-rays and neutrons are the most common probes, and each is adapted for a different context. One generally differentiates static from dynamic scattering techniques, and both will be discussed in this chapter. Static scattering like SANS or SAXS, as well as static light scattering can be treated in a common theoretical formalism. Many excellent textbooks [10, 67] exist on such techniques, and the most relevant aspects for microgel studies will be described. In addition a sub-section about photon correlation spectroscopy (often just called dynamic light scattering, or DLS) has been included.

1.2.1. Static and dynamic light scattering applied to microgels

Light scattering techniques are workhorse methods in the investigation of colloidal systems like e.g. responsive nano- and microgels. In nearly all studies of smart microgels their hydrodynamic dimension and their swelling behavior are followed by photon correlation spectroscopy. However, different flavors of static light scattering are also used to gain information about size, molecular

weight M_w, and shape of microgels. In this sub-section we will give a brief introduction to light scattering experiments and will summarize some recent works using these techniques.

1.2.1.1. Static light scattering(SLS)

In SLS the intensity of the light scattered from a microgel sample is measured as a function of scattering angle θ. θ can be converted to the magnitude of the scattering vector q by

$$q = \frac{4\pi n_0}{\lambda} \sin\left(\frac{\theta}{2}\right) \tag{1.1}$$

Here, λ is the used wavelength and n_0 is the refractive index of the solvent. For neutron and x-ray scattering the same expression can be used assuming $n_0 \approx 1$. q has the unit of a reciprocal length and as a rule of thumb $1/q$ is approximately the length scale resolution of the scattering experiment. q can be used to bring different scattering experiments to a common abscissa scale. The most straightforward way to analyze SLS data is by means of using the Guinier approximation for the form factor of the scattering particles [59] which leads to the well known Zimm equation:

$$\frac{Kc}{R_\theta} = \frac{1}{M_w \exp\left(-\frac{1}{3}R_g^2 q^2\right)} + 2A_2 c \ . \tag{1.2}$$

Here, R_θ is the Rayleigh ratio and R_g is the radius of gyration. K in eq. 1.2 is given by

$$K = \frac{4\pi^2 \left(\frac{dn}{dc}\right)^2 n_0^2}{N_A \lambda^4} \quad . \tag{1.3}$$

N_A is Avogadro's number, c is the mass concentration of the scattering particles, $\frac{dn}{dc}$ is the refractive index increment and A_2 is the second virial coefficient.

Hence, SLS can provide the radius of gyration R_g which is very helpful in expressing typical sizes of complicated objects, and it can be calculated for any known geometry of finite size. For instance, the R_g of a homogeneous sphere of radius R is $\sqrt{3/5}$ of R. Moreover, A_2 may be determined from such SLS measurements. This quantity is a measure for the interaction between the particles. Moreover, also the molecular weight of the nano- and microgels can be obtained from SLS using the Zimm equation [34, 71].

Besides the simple Guiner analysis in some cases also significant parts of the nano- and microgel form factors, $P(q)$, fall into the q range of SLS and can be analyzed by fitting the data with respective form factor models. This is nicely demonstrated in a work by Schneider et al. [96].

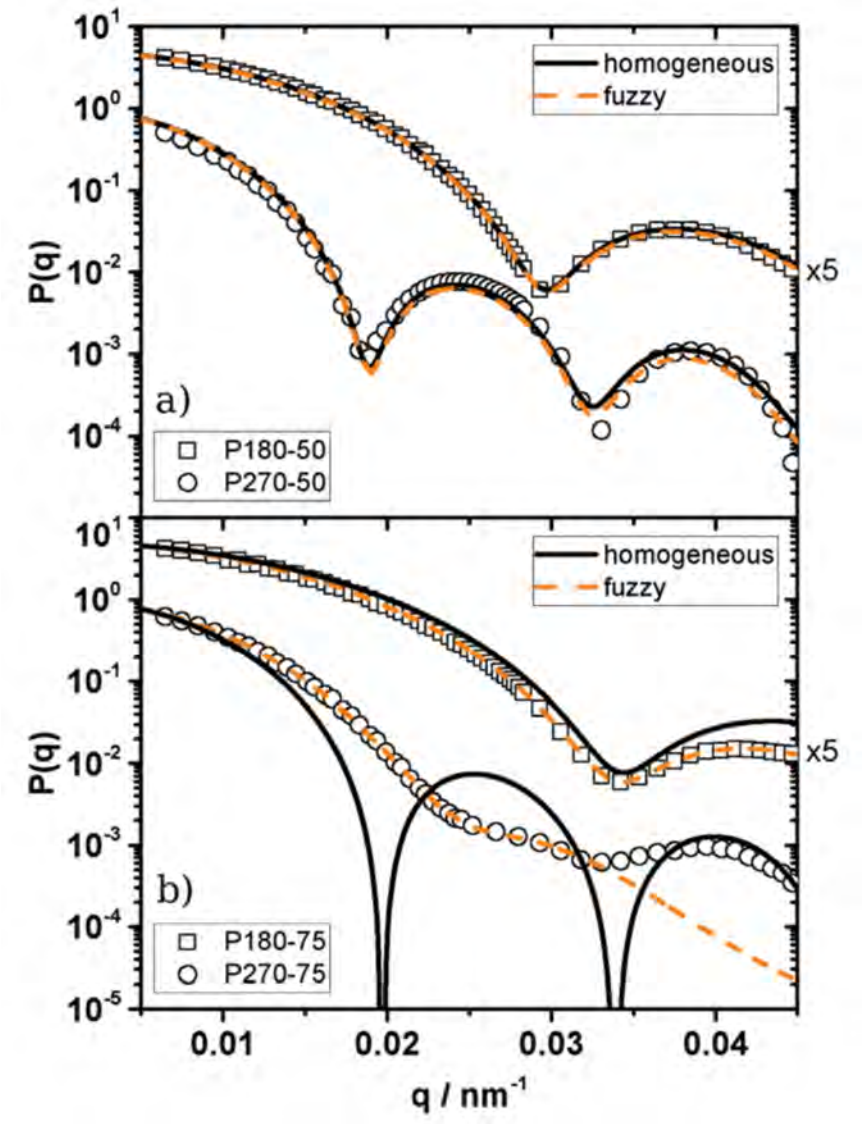

Figure 1.1: SLS data for four different microgels. The solid black lines correspond to a fit using a homogeneous sphere model. The dashed yellow lines are fits with the fuzzy sphere model. Reproduced from Ref. [96] which was published under the license CC BY 3.0 by the Royal Society of Chemistry .

Fig. 1.1 shows a comparison of the fit of SLS data using a homogeneous polydisperse sphere model with the famous fuzzy sphere form factor model for

microgels which was introduced by Stieger et al.[110] already a while ago. The different form factors corresponding to the fits shown in fig. 1.1 are given by

$$P(q) = \left[3\frac{\sin(qR_{SLS}) - qR_{SLS}\cos(qR_{SLS})}{(qR_{SLS})^3}\right]^2 \tag{1.4}$$

and

$$P(q) = \left[3\frac{\sin(qR_{SLS}) - qR_{SLS}\cos(qR_{SLS})}{(qR_{SLS})^3} \times \exp\left(\frac{(q\sigma_{surf})^2}{2}\right)\right]^2 \tag{1.5}$$

where eq. 1.4 describes the form factor for a homogeneous monodisperse sphere, and Eq. 1.5 the fuzzy sphere from Stieger et al. σ_{surf} represents the decay length of the fuzzy, hairy corona of the microgels. Note that we discuss in the Appendix the prefactor of the fuzzy sphere form factor, the deviation of which from one is important for mass determination using absolute units. In both cases polydispersity can be taken into account by convolution of the relevant $P(q)$ with a Gaussian distribution of the radius R_{SLS}[96]. Looking at fig. 1.1, it is obvious that the fuzzy sphere model leads to a better description of the SLS data. Moreover, SLS can also be used to determine the long range order and interaction between the colloidal gels. This is quantified in terms of the so-called structure factor $S(q)$ [96]. However, $S(q)$ will be discussed in more detail in the sub-sections dealing with small-angle scattering.

As already mentioned, using q as abscissa normalized absolute SLS intensities can be joined with absolute small-angle data. This was nicely shown in a recent work by Kozhunova and co-workers [59] on stimuli responsive inter-penetrating network microgels. In fig. 1.2 an example for such a joined data set is shown.

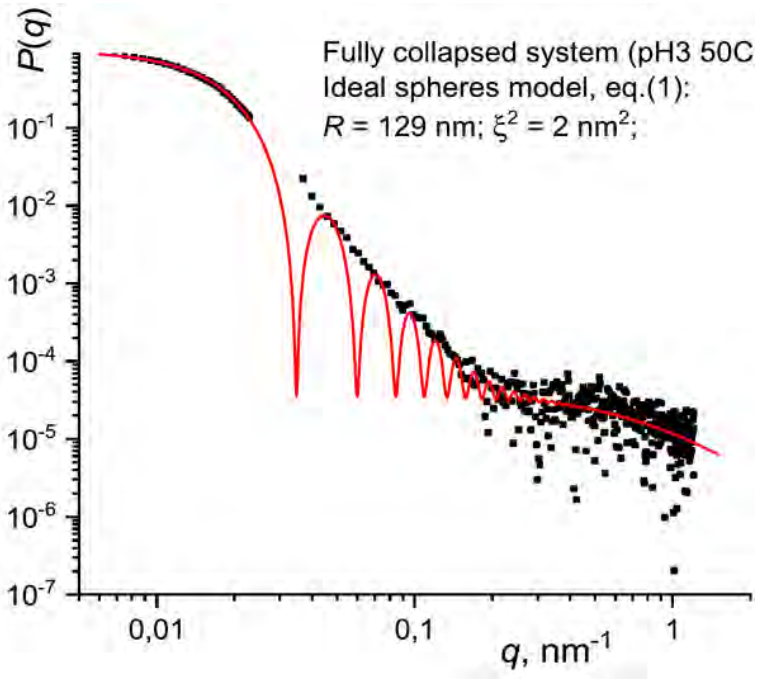

Figure 1.2: Joined SLS and SAXS data set for a collapsed microgel measured at 50 ^{o}C. Reprinted from Publication [59] with permission from Elsevier.

In this figure the series of points at low q was determined by means of SLS. The red curve represents a model which consists of the hard sphere form factor in eq.1.4 which is supplemented by an Ornstein-Zernike type contribution given by

$$I_{OZ} = \frac{I_0}{1 + q^2\xi^2} \ . \tag{1.6}$$

In this equation ξ is the local correlation length of the internal network of the microgel. In the example in Fig. 1.2, despite of being in the collapsed state, the studied system still has some "porosity", and ξ is found to be ≈ 2 nm.

1.2.2. Dynamic light scattering (DLS/PCS)

In a dynamic light scattering experiment the time-dependent fluctuations of the scattering intensity $I(q)$ are analyzed using the formalism of intensity correlation functions generated by hard wire correlators [10, 90]. This is why this method should be called photon correlation spectroscopy to distinguish from other quasi- or inelastic light scattering methods like e.g. depolarized dynamic light scattering (DDLS) which can also be done by looking at the laser line broadening in the frequency domain. The intensity fluctuations arise from the Brownian motion of the colloidal nano- or microgels in the sample solution.The standard PCS experiment yields the intensity time auto-correlation function $g_2(\tau)$ which can be converted into the time auto-correlation function of the electric field $g_1(\tau)$ using the Siegert relation

$$g_2(\tau) = 1 + |g_1(\tau)|^2 \quad . \tag{1.7}$$

Here, τ is the sample time. For ideal monodisperse samples the function $g_1(\tau)$ is a single exponential decay of the form $g_1(\tau) = \exp(-\Gamma\tau)$ and the relaxation rate Γ can be used to compute the translational diffusion coefficient D according to $\Gamma = Dq^2$. This also indicates that a plot of Γ vs q^2 yields information about the type of motion which is effectively observed in a PCS experiment. If such a plot results in straight lines through the origin, this reveals that the experiment only "sees" center-of-mass diffusion of the colloidal gels. For most colloidal gels this is fulfilled and a recent example is shown in fig. 1.3.

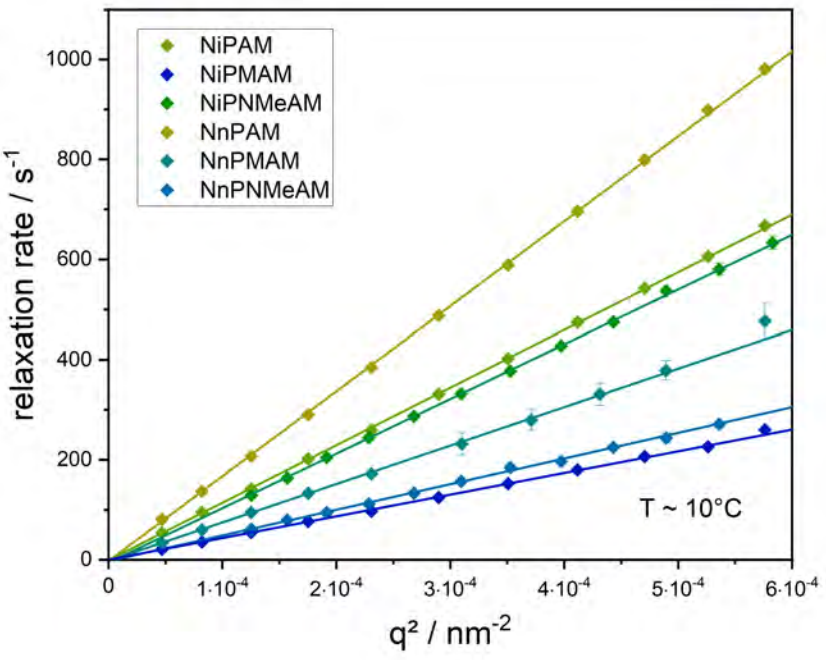

Figure 1.3: Averaged relaxation rates Γ for a series of homopolymer microgels made with alternative monomers [44] at $T = 10$ °C: swollen state. Each correlation function was measured three times at 11 scattering angles. For all particles, the data follow the expected linear behavior indicating purely diffusional dynamics. Within the experimental precision all fits go through the origin. Reproduced from ref. [44] under the license CC BY-NC 4.0.

Fig. 1.3 shows data for the already widely used and commercially available monomers *N*-isopropyl acrylamide (NiPAM) and *N*-isopropyl methacrylamide (NiPMAM), as well as for the rarely used acrylamides, N,n-propylacrylamide (NnPAM) and *N*-*n*-propylmeth- acrylamide (NnPMAM), and the previously not used monomers *N*-isopropyl-*N*-methylacrylamide (NiPN- MeAM), *N*-*n*-propyl-*N*-methylacrylamide (NnPNMeAM). Usually the polydispersity of microgels is rather low and the decay of the correlation functions nearly follows a single exponential. However, in case of higher polydispersities $g_1(\tau)$ has to

be described by a weighted sum of exponentials

$$g_1(\tau) = \int_o^\infty G(\Gamma) \exp(-\Gamma\tau)\, d\tau \quad . \tag{1.8}$$

The relaxation rate distribution function $G(\Gamma)$ can be obtained by numerical Laplace inversion of $g_1(\tau)$ [85, 97] or by using the method of cumulants [58, 37]. In both cases a mean value for Γ is obtained.

The slope of the straight lines in fig. 1.3 is the translational diffusion coefficient of each microgel. Knowing D the hydrodynamic radius R_h is computed via the Stokes-Einstein equation:

$$D = \frac{kT}{6\pi\eta R_h} \tag{1.9}$$

As stated before, in most studies of microgels R_h is measured at different temperatures crossing the volume phase transition temperature (VPTT) of the particles. A recent example for the outcome can be found in a work by Freeman and co-workers[35].

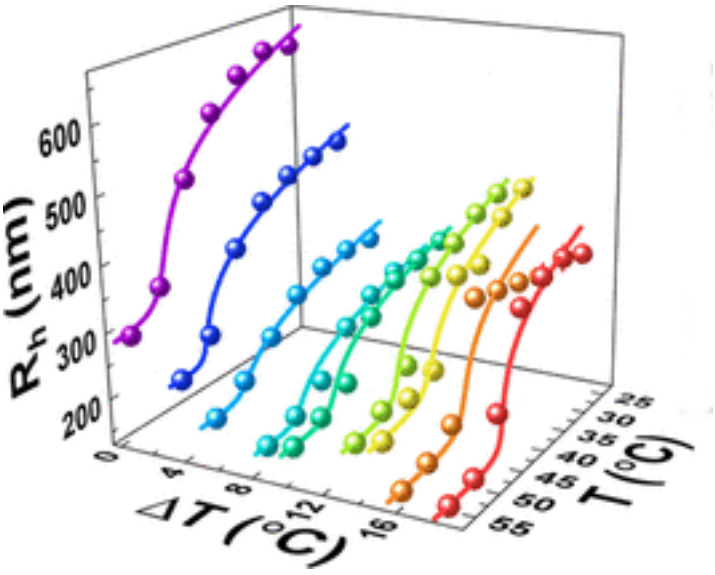

Figure 1.4: Swelling curves of polysaccharide microgels as measured by PCS. ΔT indicates the difference between the synthesis temperature and the LCST of the microgels. Obviously the swelling behavior is impacted by ΔT. Reprinted with permission from [35]. Copyright 2020 American Chemical Society.

Fig. 1.4 shows the swelling curves for rather unusual polysaccharide based microgels which also exhibit a volume phase transition like their polyacrylamide counterparts.

At several large scale facilities PCS can be used to follow microgel samples in-situ during small-angle neutron scattering experiments [75, 94]. Small-angle scattering experiments will be discussed in the following subsection.

1.2.3. Small-angle neutron and x-ray scattering applied to microgels

In this subsection we will focus on the specific application of SANS (and SAXS) to unravel the structure of microgels suspended in solvents. The fundamental scattering process of neutrons (or X-rays photons interacting with electrons, a valid analogy throughout this text) is the creation of a spherical secondary wave by the presence of a nucleus hit by an incoming wave. The latter is created in the heart of a nuclear research reactor, or in a spallation source, and transported and directed conveniently towards the sample by experimental installations like guides, collimations and wavelength selectors, which we will take for granted in this introduction. In the end, a planar wave of wavelength λ hits the sample, and is mostly transmitted without change in direction, sadly ending its short life on a beam-stop. Some of the neutrons, however, are scattered laterally under the form of the above-mentioned secondary waves, they thus leave the direct beam, and can be collected on a detector. These neutron waves coming from different nuclei in the sample interfere, and the detector thus shows an intensity pattern resulting from such interferences. The latter depending on the phase of each neutron, and thus on the distance the neutron has travelled, the intensity pattern encodes the distance distribution between nuclei in the sample.

The fundamental problem of the scientist analyzing such data is thus to work his/her way back from the intensity pattern to the distance distributions, and thus to the microstructure of the samples. This is much more difficult than looking at an electron micrograph, but it contains valuable information. In par-

ticular, all the distances in the sample are averaged, and one thus does not only look at a very small sample portion as in a TEM picture. Scattering provides thus intrinsically an ensemble average, which is both an advantage (because it minimizes artifacts), and a disadvantage (because it only gives averages, e.g. over size distributions). And it is also considerably more complicated ...

In order to fully understand how microgel particles can scatter, one needs first to revisit the elementary scattering process. When writing down the equation of the spherical secondary wave, a prefactor describing the power of the interaction is needed. This prefactor has the unit of a length, and it is called the (coherent) scattering length b of the nucleus causing the process. It is not only specific to each element, but also to each isotope. This implies that we can differentiate isotopes in the sample, which is one of the greatest features of neutron scattering. Indeed, replacing, e.g., a "normal" polymer (i.e., made of protons, like in polyethylene, -CH_2-), by its deuterated counterpart (-CD_2-) leaves the chemistry mostly unchanged, but totally modifies the scattering. By using deuterated and hydrogenated polymers (possibly within the same chain, e.g. to label and thus locate chain ends), it is thus possible to see which one is where. In small-angle neutron scattering, one is usually interested in the overall, supra-molecular structure of objects. The individual scattering length b of each nucleus is then regrouped and expressed as a scattering length density given by the sum of all the b's in a volume, divided by that volume. A typical volume may be a chemical repeat unit. The interested reader should look up the coherent scattering lengths of H, D, and O, and calculate the scattering length densities of H_2O and D_2O (-0.5×10^{10} cm^{-2}, and 6.4×10^{10} cm^{-2}, respectively). This little exercise shows that changing the solvent is a way to completely change what is seen by the neutrons. The corresponding technique

is called contrast variation, and an example is shown in Figure 1.5.

In Figure 1.5, the scattering length density of the solvent water is varied by mixing light and heavy water, and the polymer is seen to have a varying visibility in each solvent, expressed by the square- root of the scattered intensity in some (small-angle) direction. The most important feature in Figure 1.5 is that the scattered intensity vanishes at a given H_2O/D_2O ratio, which is called the match point. Here the scattering length density of the polymer is exactly equal to the one of the water mixture, i.e. we have actually measured it, and thus also its density (i.e., volumetric mass) within the solvent! If this polymer is now part of an assembly, it can be seen for mixtures far from the match point, and it will be invisible at the match point. It is good practice in neutron scattering experiments to start with a contrast variation of each ingredient, and compare it to values expected on the basis of the chemical sum formula. As a result, the relevant quantity is the scattering contrast, i.e. difference in scattering length density between the object and the solvent (or matrix):$\Delta\rho = \rho - \rho_{solv}$. In Figure 1.5, we have also shown in the bottom inset the contrast variation for a D-polymer, and in the sketch an artist view of the visibility of a particle made of H- and D-polymer, in various solvent mixtures. Towards the right, the H-shell is matched by the mostly H-solvent, and towards the left, the inverse is true. Contrast variation thus serves to highlight specific parts of the particle if isotopic substitution can be performed chemically.

If we now measure the entire scattered intensity collected by the detector (or sets of detectors to cover wider angles), we obtain a function of the magnitude of the scattering wave vector q. Examples of intensity are shown in Figure 1.6. Technically, $I(q)$ is a scattering cross section of the sample per unit volume, which is why its units are cm^{-1}. Once this measurement is done correctly - this

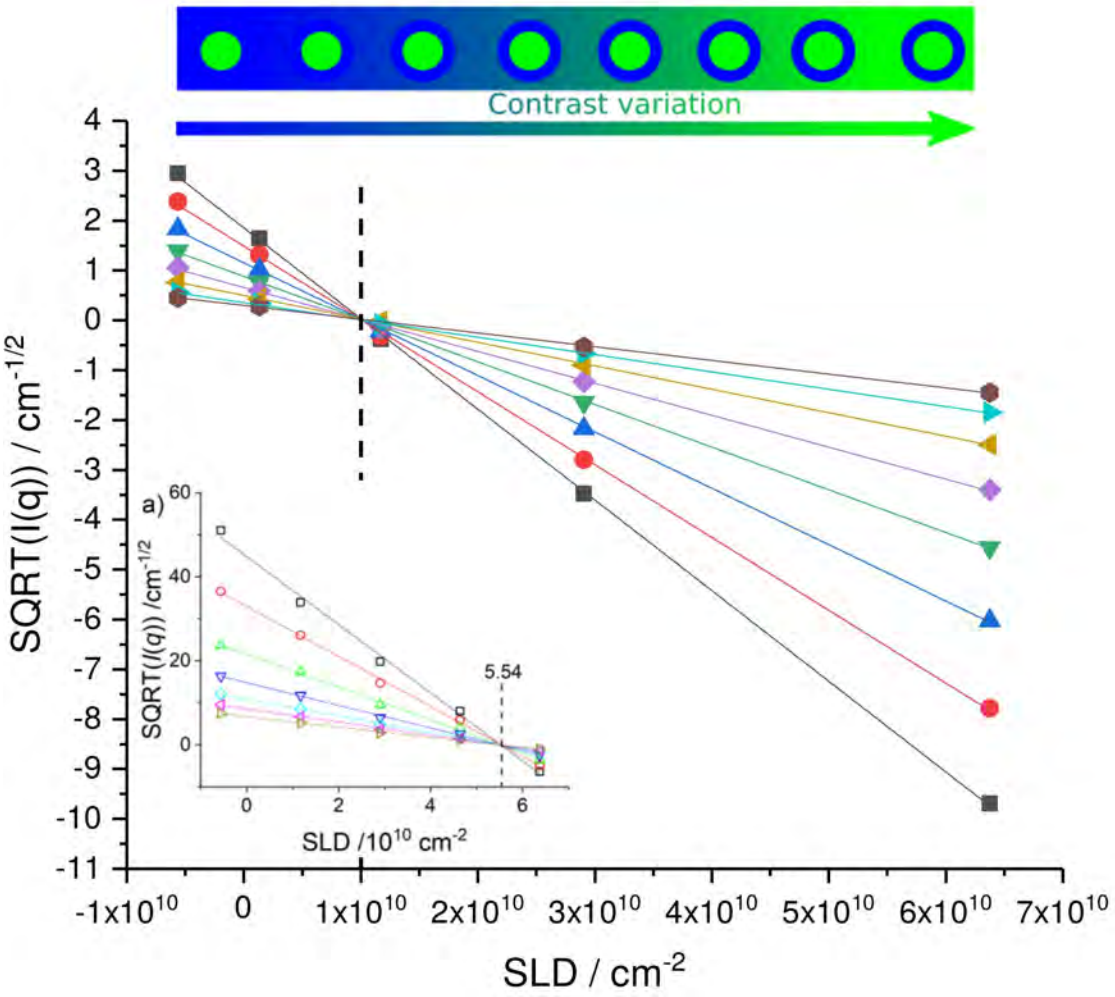

Figure 1.5: Contrast variation for several q-values. Inset: D-polymer. Sketch: visibility of D-core and H-shell in varying solvent mixtures. Adapted with permission from [22]. Copyright 2018 American Chemical Society.

implies a little extra work, like exactly knowing the contrasts, concentrations, measuring transmissions and incoherent backgrounds, etc. - the happy scientist can start thinking about the micro-structure of this sample.

In Figure 1.6, three intensities have been superimposed, corresponding to the same pNNPAM microgel at different temperatures – shifted vertically for clarity. At the highest T, the particles are collapsed and do not interact: form factor scattering is observed, corresponding to the Guinier plateau followed by oscillations caused by interferences due to the well-defined particle geometry. As the particles swell with lower T, oscillations weaken, and steric interactions set in, leading to the structure factor effect at low q. Such interactions can be studied and described. They are interesting, e.g., if one wished to study squeezing of microgel particles [103].

Due to lack of space, we cannot focus on structure factors here, and only introduce some basic notions. The fundamental concept is the one of spatial correlations, which are the result of interparticle interactions. For hard spheres, e.g., the evolution of the low-q limit of $S(q)$ is well described by the Carnahan-Starling equation [46], and the entire function has been determined from integral equation theory, using the Percus-Yevick closure [15]. On the other hand, highly repulsive long-range interactions, like electrostatic ones, lead to ordering of the suspension. Suitable solutions of the integral equations exist in the literature, like ref. [45]. The corresponding particle-particle correlation function then adopts a characteristic shape, usually peaks, which translate into peaks in the scattered intensity. Here a simple rule can often be used: $\frac{2\pi}{q_0}$, where q_0 is the 1st order peak position which gives the size of a cubic box containing one particle. Using volume conservation, it is thus possible to estimate the dry volume of the particle from a structure factor measurement. Repulsion also

leads to a depression of the low-q intensity. Other interactions, like attraction inducing aggregation, typically lead to low-q increases, which can be interpreted as mass increases. It is thus possible to follow interactions by focusing on the low-q scattering, e.g. in terms of the second virial coefficient at high dilution. Alternatively, one may focus on the shape of the entire function, if models are available for comparison, like, e.g., for fractals [112]. Coming back to pure form factors, the usual method of measuring microgel particles only (i.e. without being perturbed by their interaction) is to lower the concentration and check that two successive measurements give the same $I(q)/\phi$. We have insisted on the unit of the intensity because knowing $I(q)$, one says in absolute units allows one to exploit the low-q limit $I_0 = I(q \to 0)$. The scattered intensity then reads at low angles:

$$I(q) = I_0 \exp\left(-\frac{q^2 Rg^2}{3}\right). \tag{1.10}$$

$$I_0 = \phi \Delta\rho^2 V_{dry} \tag{1.11}$$

Eq. 1.10 is called the Guinier approximation, and it is valid (see Fig. 1.6) at low angles in absence of interaction. It also corresponds to the low-q version of eq.(1.4), or equivalently to eq.(1.2) with $A_2 = 0$. The Guinier law gives the radius of gyration R_g, which describes the average spatial extent of the objects and has been introduced in section 1.2. In eq. 1.11, we have given the low-q limiting value, it is proportional to the volume fraction of objects, to their dry volume V_{dry}, and to the square of their contrast. This square is the reason for plotting the square root of the intensity in Figure 1.5.

The dry volume deserves some further comment. We have chosen to identify the object by its chemistry. Imagine a thin hollow shell made of dry polymer,

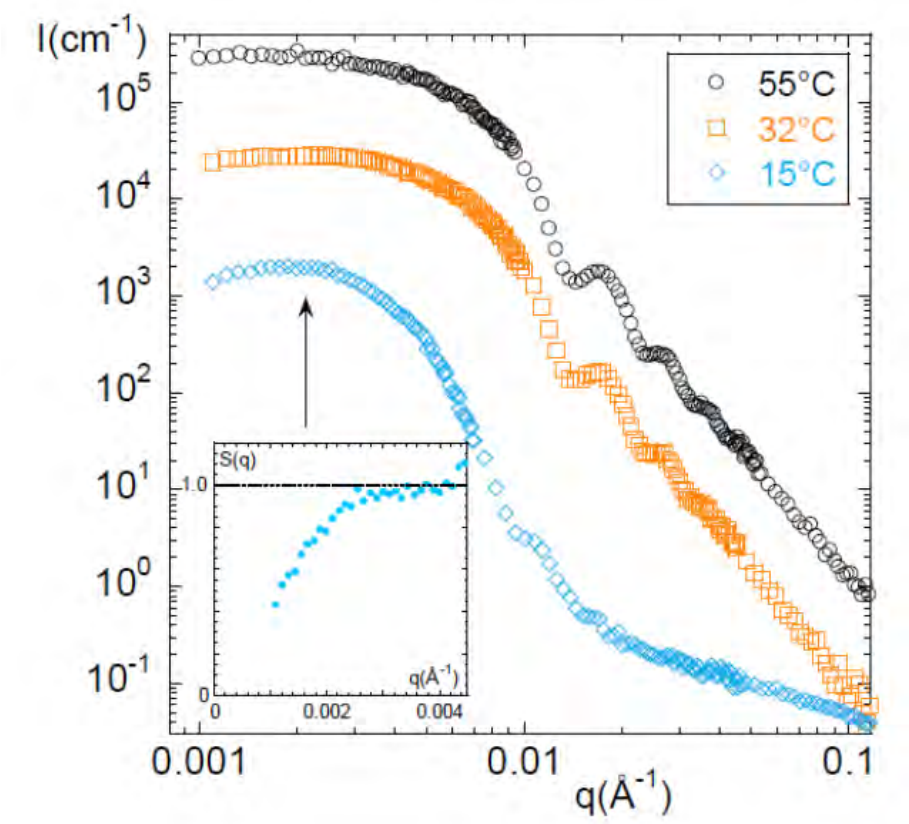

Figure 1.6: Structure of pNNPAM microgel in D_2O for three different temperatures as indicated in the legend. The SANS intensities at 32^oC and 55^oC have been vertically shifted by a factor of 10 (resp. 100). In the inset, an estimate of the structure factor is shown for the lowest temperature.

with solvent in the core. The total object contains water and polymer, but V_{dry} only refers to the polymer part, ϕ only to the polymer volume fraction, and $\Delta\rho$ to the dry polymer contrast in water. The amount of polymer matter in the object can thus be compared to their spatial extent given by R_g. For a thin shell, R_g is given by the shell radius. Comparing V_{dry} to R_g thus gives a hint on how much matter is distributed where in space, and one can start imagining geometric models consistent with these two (independent!) measurements. The simplest one could be a hydrated sphere: R_g can be converted into a sphere radius R, of (wet) volume $\frac{4\pi}{3}R^3$, and the latter compared to V_{dry}, the ratio giving the hydration. Below, we will discuss an in principle similar approach to internal microgel concentration profiles, where the two ingredients, local concentration at a given distance from the center, are resolved. As a last point, let us mention that particles are usually polydisperse, and polydisperse expression involving moments of the size distributions are readily available for eq. 1.11, see for instance ref.[78].

Up to here, we have concentrated on the low-q scattering, which according to the q^{-1}- argument encodes the average large-scale structure of the microgel particles, i.e. global spatial extent and total (dry) mass. Of course, much more information is available: the form factor scattering in Figure 1.6 can be analyzed as a function of q. Going to higher q is equivalent to increasing the magnifying power of a microscope. In the intermediate q-domain, spherical particles usually display oscillations related to their size, and the damping of these oscillations indicates how homogeneous, monodisperse, and well-defined the particles are. At the highest q, a power law is usually found. In the case of microgels, it extends typically between a shallow q^{-1} power law characteristic of linear chains, some intermediate fractal statistics of chains, e.g. $q^{-1.7}$

for chains in good solvent, or q^{-2} for ideal chains, up to q^{-4} (Porod decay) when all the chains collapse smoothly onto the particle and only a sharp interface remains. However, it can not be ruled out that especially the collapse of dangling ends at the surface of the microgels might lead to some surface roughness. This can be modeled by using modified Porod decays [61]. Measuring these power-laws thus provides indications of the chain statistics, which in the case of microgels are strongly temperature-dependent. Several expressions exist in the literature for chain scattering, the best-known one being the Debye equation for ideal chains [30]. The latter can be generalized to any power law if needed [43]. Depending on the total size of the microgel particles, the polymer network may also contribute characteristic scattering features. Indeed, due to fluctuations in cross-linking density, density fluctuations may be visible, as well as the network mesh size. The reader is referred to the relevant literature for details [63].

Once one knows the amount of matter to be distributed on average within microgel particles (via V_{dry}), their average spatial extent (R_g), and the local conformation of the chains making up the network, one is left with the question of the internal concentration profile of the microgels. There are essentially two approaches to this problem. The first one is called model fitting, and it consists in starting from a hypothetical model structure (e.g. a homogeneous sphere of radius R). The form factor of such an object is analytically known, and one can thus adapt R until the theoretical intensity describes well the measured one. Due to the mysteries of scattering, one can then state that microgels may be homogeneous spheres of radius R. In reality, one can never be completely sure, but if the dry volume, the R_g, the shape with its oscillations coincide, one may be pretty sure to have chosen the right model.

In the literature, several models have been proposed to describe microgel scattering: fuzzy spheres as discussed in 1.2 introduce a soft decay on the edge of the spheres [110, 9], and other models have been discussed by us [22], including an expression based on a Flory-Rehner approach by Boon and Schurtenberger [14]. The essence of all these models is that if they are chosen correctly, then the fits are good, and the structure is resolved. And it is the experimentalists job to choose the right model.

We have recently applied a more general approach, where no geometry is a priori imposed, besides that the spherical symmetry of the objects, as well as their polydispersity, is known beforehand. Such a free-form analysis has been applied to block-copolymer micelles [66], and later to microgel particles [115, 22]. The method is based on a reverse Monte Carlo algorithm, which searches stochastically for the best fit of a multi-parameter model given by the concentrations in successive spherical shells. The concentration in each shell thus defines the average density profile of the particle, from the center to its surface. It is thus not much different from the above model-fitting, only that (many) more parameters need to be optimized. Such approaches are nonetheless known as inversion techniques, as they invert the intensity back into structure, whereas a model fit assumes a structure and compares to intensity. Inversion techniques are part of a larger class of techniques, like the (deterministic) indirect Fourier transform and its variants [42, 41], and (stochastic) reverse Monte Carlo calculations [69]. The difference here is that the concentration profiles are based on real monomers moving between the shells in order to optimize the fits, and that the spherical symmetry is implemented from the beginning. The physics of the problem is thus taken into account from the construction of the method, as it is done in other fields where

the basic building blocks like nanoparticles are used [79, 72]. This means of course that for each problem, a new algorithm has to be set up. Finally, as all such methods, they suffer from under-determination. In such so-called ill-posed problems, more than one solution exist. The standard way is to favor a solution by regularization, e.g., by demanding that the profile decays smoothly, and average over families of solutions obtained in the course of a simulation.

The geometry of the multi-shell model is defined by the number of monomers in an average particle consistent with eq.(1.11), taking into account the cross-linkers and particle polydispersity in all calculations. These monomers are distributed over N_p shells, where N_p is typically 30, of width $\Delta R = 2$ nm for our particles, but this needs to be adapted to the particle size. Obviously, certain physical bounds need to be respected, like the minimum occupation of a shell (no monomers in a shell), but also the maximum filling (100% volume fraction). The idea of the algorithm is to start from some initial condition, which may be having all shells filled from the center of the particle until all monomers have been distributed. This initial condition should be varied in order to check the convergence of the procedure. The volume and number of monomers in each shell may be transformed into the scattering length density of each, and then the sum of each contribution may be calculated in order to obtain the total intensity:

$$I_{shells}(q,r) = \sum_{i=1}^{N_p} \frac{N}{V} \left[\frac{4\pi}{3} r(i)^3 \left(\Delta\rho(i) - \Delta\rho(i+1)\right) 3 \frac{\sin(qr) - qr\cos(qr)}{(qr)^3} \right]^2 \tag{1.12}$$

Here, N/V is the number of microgel particles per unit volume, r is the outer radius of each shell $r(i) = i\Delta R$, and $\Delta\rho(i)$ is the scattering length con-

trast of shell i. The contrast of the surrounding solvent shell $\Delta\rho(N_p + 1)$ is set to zero. The Monte Carlo part is then to modify the distribution of the monomers between the shells, e.g. by moves of some of them between randomly chosen shells (respecting the bounds), and check if the outcome of eq. 1.12 agrees better with the experimental scattered intensity. Here, agreement is usually expressed in terms of χ^2, i.e. a normalized sum over squares of differences between the prediction I_{shells} and experiment, modulated by some error bar. Moves leading to decreasing χ^2 are always accepted, but in order to explore also some less satisfying monomer profiles in a so-called simulated annealing approach, slight increases of χ^2 may also be accepted. This latter process is driven by an effective temperature parameter χ_T, which in the beginning accepts large χ^2- increases, and progressively diminishes this amplitude. As a last point, the result needs to be regularized as outlined above, which amounts to a simultaneous optimization of the agreement with the experimental intensity (low χ^2), and high smoothness.

In Figure 1.7(left), the progression of the algorithm from the initial condition to the final outcome is shown. The black squares show the evolution on a logarithmic scale of χ^2 with the number of Monte Carlo steps. It is found to be satisfying after a few hundred thousand steps, and then all parameters are kept fixed and the solution is averaged. In the course of the annealing process, the effective temperature χ_T is seen to be pushed down until it is kept constant in the averaging phase. Simultaneously, the number of monomers N_{move} tentatively moved in each MC step is also decreased. While the simulation is running, the roughness of the profile stays under control (see original article). In the inset of Figure 1.7(left), the experimental intensity to be fitted is shown, with the initial guess, and the final fit superimposed to the data.

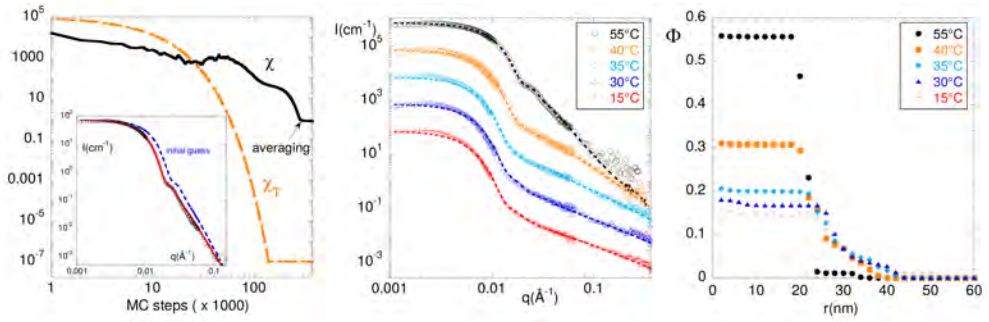

Figure 1.7: Structural analysis of a pNIPMAM core in D_2O. (left) The decrease of χ^2 as a function of the number of Monte Carlo steps, up to the moment when averaging is started. The process is driven by an effective temperature χ_T. The inset shows the improvement of the fit starting from the initial guess. (middle) Intensities as a function of wave vector for a temperature series, shifted vertically by powers of 10 for clarity. The fit functions are superimposed. right) The radial density profiles corresponding to the RMC-solutions shown in the mid panel. Adapted with permission from [22]. Copyright 2018 American Chemical Society.

In the middle panel, Fig. 1.7(middle), the intensities for the same microgel particles are shown for various temperatures, together with the best RMC-fit. In the right panel, Figure 1.7(right), finally, for each T the resulting profiles are shown for this p(NIPMAM) microgel, which afterwards is used as the core in subsequently studied core-shell microgels (see section 1.3). This is thus the real-space signature of the microgels as seen by small-angle scattering analyzed through the multi-shell model. The profiles give simultaneous information on the local density and spatial extent, the two being coupled by volume conservation. At the highest temperatures, dense and small cores are thus found, whereas swelling leads to much more diffuse, tenuous structures.

1.3. Multicompartment and multi-stimuli responsive microgels

The thermoresponsiveness of microgel particles is only one of available smart properties. Sometimes the sensitivity to other stimuli, possibly within the same object, is of interest for fine-tuning morphologies, colloidal stability, and interaction with guest molecules. Introducing electrostatic charges within the microgel is an obvious choice, and copolymerization with ionic or ionizable monomers is a straightforward way to make the backbone carry charge, possibly with a pH-dependence as with for instance weak acids, which are neutral below their pK_a, and negatively charged above. The main principles of microgel response to electrostatics are that the pH can act as a trigger to switch on charges, the effect of which is possibly compensated by mobile ions screening electrostatic interactions on the scale of the Debye length. The ionic equilibrium between counterions and the charged backbone is governed by a compromise between electroneutrality and translational entropy of ions, and the resulting average spatial distribution of ions is described by the Poisson-Boltzmann theory - or Debye-Hückel in its linearized version. This results in swelling of the microgel by the osmotic pressure of the counter-ions. This swelling effect is thus both pH- and ionic strength-dependent.

Having different stimuli at hand, the next step in complexity is then to design multicompartment-multistimuli microgel particles, with a different thermosensitivity for each compartment. From the synthesis conditions of precipitation around nuclei, spherical symmetry emerges naturally, and multicompartments of different swelling properties are conveniently characterized by shell-like structures [47], the radial density profiles of which can be extracted

from scattering profiles.

Density profile analysis of isotropic structures turns out to be a powerful method both for simple microgels (like pure crosslinked pNIPAM), where the cross-linking density varies with the radius due to the different reactivities of the cross-linker and the monomer, and purpose-synthesized hollow-shell, particle-shell, and other core-shell microgel particles.

Hyatt et al. have proposed a study of pNIPAM co-polymerized with relatively high amounts of acrylic acid (24%mol) [52], complementing a previous study where the acid groups remained neutral at low pH [51]. At high pH and high temperature, pNIPAM deswells, while partially ionized acid groups tend to swell following the entropic pressure of the counterions. This competition leads to an electrostatically driven microphase separation with a dense core and a tenuous shell. This particular structure has been evidenced by light scattering, PCS providing the hydrodynamic radius R_h sensitive to the soft shell, and SLS the radius of gyration R_g, i.e. a measure of the mass distribution in space. Data are analyzed with a polydisperse fuzzy sphere form factor which these authors refer to as core-shell due to the fuzzy surface; at higher q, a standard polymer network term is included, which we will not explicitly mention in all work discussed here. As a result, R_g/R_h is observed to become quite small (below $\frac{1}{5}$), indicating that most mass is concentrated in the center of the microgel and thus forming a dense core. Simultaneously, a decrease in mesh size accompanies the R_g/R_h decrease above the volume transition temperature. These findings are similar to the internal phase separation observed by Wu et al. [121], who synthesized microgel systems with ionic liquid comonomers. In their case, however, the alkyl side chains are distributed across the entire particle, and TEM

micrographs and DSC show the formation of spherical crystalline mesophase zones exhibiting a radius in the 10 nm range, inside the particles. This might have been a promising system for a complete analysis of the total small-angle scattering, as done in a first system of the Richtering group some years ago [55]. The latter authors had added a local spherical term to the intensity model in order to account for what they call with an imaginative picture "dirty snowballs".

An example of control of the colloidal stability via the addition of reactive macromolecular stabilizers has been provided by Etchenausia et al. [31]. This group has studied PVCL-based microgels and could show that an outer cationic stabilizing shell is formed, without losing temperature sensitivity. SANS fits with a sphere model at low q confirm the DLS results of swelling with T and surprisingly also with total concentration. It remains to be clarified to which extend aggregation modifies the scattering signatures.

By adjusting both ionic stimuli – pH and ionic strength –, the morphology of microgels can be controlled as shown by Bergman et al. [8]. These authors have copolymerized acrylic acid and NIPAM, and they show that they can target swelling of the core and of the shell made of dangling ends by playing with both stimuli. Very nicely resolved static light scattering data including higher order form factor oscillations allow inverting the scattering profile into a density profile using Mie theory relevant for big objects which strongly scatter light. This procedure is also backed up by form-free modeling in a analogous way [115], as outlined for our own contributions below [22, 86, 66]. In parallel, PCS data gives access to the hydrodynamic radius, and thus to the extension of the shell into the solvent. The same group has previously set up a Flory-Rehner-

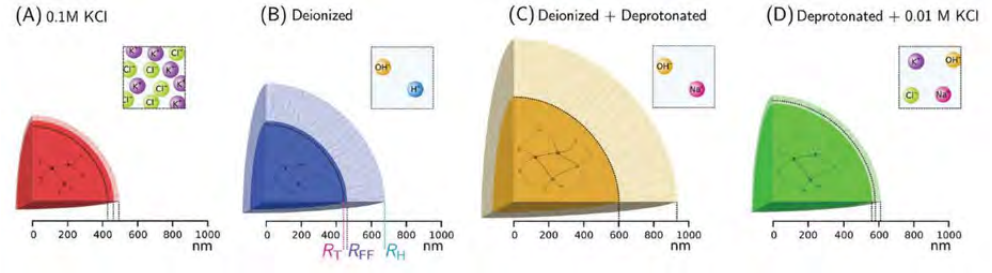

Figure 1.8: Radial measures of ionic microgels, indicating the swelling of the core and the corona in various ionic environments fixed by resins and salt. The figures (AD) correspond to different conditions. The core radius R_{FF} as determined from SLS, as well as the hydrodynamic radius R_h from PCS are shown, differences between them are used as a measure of the dangling-end contributions. Reproduced under license CC BY-NC 3.0 from ref. [8].

based model accounting for the effect of cross-linking gradients on the microgel shape as seen by the density profile [14]. Here, they add an electrostatic osmotic pressure term to their model, and show that it captures successfully the effect of the ionic stimuli. In particular, deionization induces shell swelling due to the reduced charge screening without affecting the core, whereas deprotonation by increasing the pH makes the core swell by a factor of two under the pressure of the counter-ions. Adding salt again at this high pH leaves the core swollen, but collapses the corona because the latter has a higher sensitivity to salt due to the lower density of backbone ions. This sequence of behavior is depicted in Figure 1.8, illustrating the effect of each stimulus individually.

In traditional pNIPAM microgels, the non homogeneous cross-linking density is a major property influencing the particle morphology. This is not necessarily always the case, as shown for another system by Schneider et al. [96], the analysis of which has been used above to introduce form factors (Fig. 1.1). This group has varied the cross-linking density of polystyrene particles by a

factor of ten, screening the range from soft pNIPAM-like behavior to hard spheres. The similar reactivity of the cross-linker and the styrene makes these particles homogeneous, free of any cross-linking gradient. These authors are mainly interested in colloidal glass transitions, and proceeded therefore in a mapping of these spheres of increasing softness onto the hard sphere phase diagram via the observation of $S(q)$. Only at the lowest cross-linking ratios, weakly fuzzy spheres have been observed by static light scattering, as shown by their rigorous study of form factor scattering in the limit of the lowest possible concentrations. Finally, fuzziness could also be tuned by reaction conditions, which was initially varied to ensure low polydispersity. The corresponding scattered intensities are shown in Figure 1.9, where the fits with homogeneous or fuzzy spheres are seen to be more and more differentiated as the monomer-cross-linker feed time is increased, indicating growing fuzziness.

Unlike the formation of fuzziness sometimes referred to as corona structure caused by the inevitable cross-linking gradient, purpose-designed core-shell microgels with true double thermoresponsiveness have been developed in the past few years. Brugnoni et al. have set up a system based on a hard silica core, which can be dissolved after shell synthesis in order to obtain hollow microgels [16]. They have subsequently polymerized two shells, the inner with pNIPAM, and the outer one with pNIPMAM which has a ca. 10 K higher volume transition temperature, for a typical swollen size of 250 nm characterized by dynamic light scattering. The systems are thus silica-shell-shell, and hollow-shell-shell, while moreover the outer shell can be left out for comparison. Besides cryo-TEM, SANS is used to access the polymer density profiles, taking advantage of the solvent H_2O/D_2O to match the silica contribution if present. Core-multishell modeling with inter-penetrating interfaces and outer

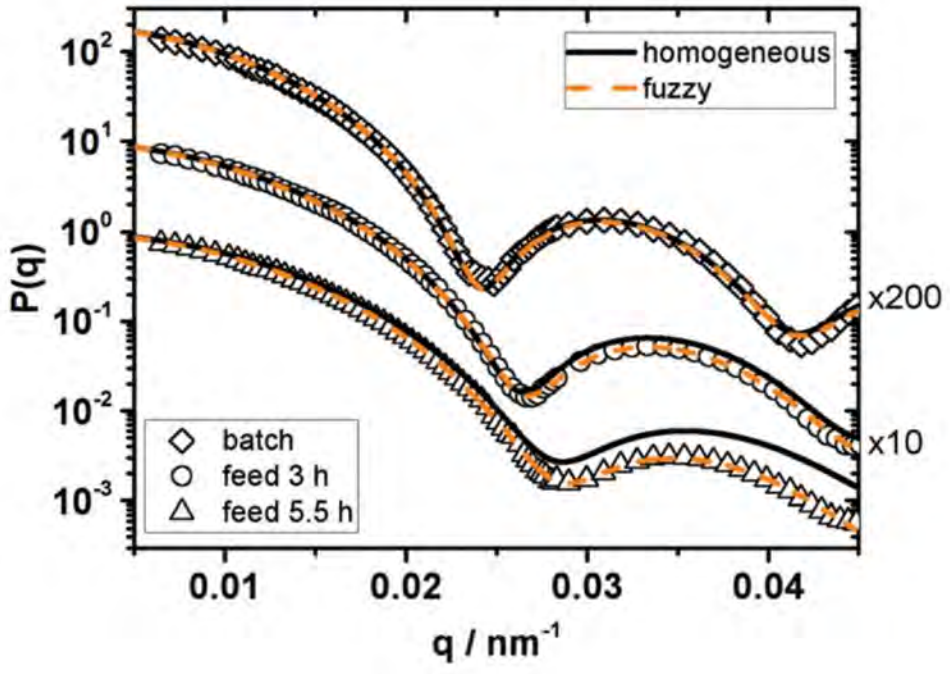

Figure 1.9: Comparison of the experimental form factors of three different samples of 1:75 cross-linked polystyrene microgel particles in the good solvent toluene. The diamonds represent the data for a sample made by standard batch synthesis. The other two data sets correspond to semi-batch synthesis with two different monomer feeding speeds. Slower feeding leads to increased "fuzziness" of the PS particles. For easier comparison P(q) was multiplied by the factors indicated on the right side of the figure. Reproduced from Ref. [96] with permission of the Royal Society of Chemistry.

fuzziness, which moreover is compared to computer simulations, provides density profiles. Their analysis provides the keys to understanding the impact of constraints within such doubly thermo-responsive microgels, which the authors refer to as push-pull effect. Indeed, attachment of the inner shell to the silica core limits swelling, and in this case inter-penetration with the outer collapsed shell is observed. On the contrary, swelling is more pronounced for the hollow core, which is partially filled upon heating, avoiding shell inter-penetration.

Also, PCS shows that the outer shell constrains the inner one between the two T_c, when the inner shell starts swelling, a phenomenon referred to as corset effect and which has attracted further attention as discussed below. In all cases, however, the interaction between the two shells has the effect of preserving the cavity, a case which may be compared to the inverted system studied by the same group before, with the outer shell swelling first upon heating [93]. The microgels with a collapsed inner and a swollen outer shell showed similar density profiles with and without silica core, with a slight increase of the cavity size. In the context of such studies, one may mention that most conclusions (like inter-penetration) are drawn by comparison of the total density profiles. One should keep in mind that in absence of deuteration, SANS is not capable of differentiating between the two monomers. Some usually plausible assumptions are thus necessary for data interpretation.

In a very recent article, Brugnoni et al. [18] study hollow double shell microgels designed in order to release possible guest molecules from the cavity by swelling of the shell, thereby providing permeability via the increase of the mesh size. Their system is based on pNIPAM co-polymerized with an ionic monomer in the inner shell, thereby lowering the transition temperature to below room temperature. They show by static light scattering via the radial density profiles obtained with a fuzzy core shell model that the cavity remains preserved, while colloidal stability is maintained even in the shrunken state. Indeed, at room temperature where the pores towards the cavity are more closed in order to localize potential guest molecules, the steric protection of the outer and swollen pNIPAM shell remains effective.

Adding a new trigger is not always the only reason for introducing ionizable comonomers of weak acids. The same pathway has been explored by Wypysek

et al in order to circumvent the problem of too low T-responsiveness of highly cross-linked hollow shells, whereas too loose cross-linking introduced floppiness and did not preserve the hollow cavity [122]. As with the above-mentioned systems, the pH then controls if the system is responsive to temperature in the neutral state. In case of backbone ionization, here of co-polymerized itaconic acid at 10 mol%, at high pH sensitivity to ionic strength is introduced. The advantage of this molecule is to maintain colloidal stability of the silica during synthesis, as it can be copolymerized in the neutral state. The main effect of the backbone charge present at high pH is to add counter-ion osmotic pressure in the system, which acts as a radial force towards the outside, thus preserving the cavity. In this context, a Poisson- Boltzmann cell model has been set up to investigate the ionic profiles and resulting pressures. The corresponding scattering data has been analyzed by a fuzzy core-shell model. The first result of the introduction of the ionic stimulus is the suppression of thermo-sensitivity in the relevant temperature range. In the charged state, the system becomes sensitive to ionic strength. Screening by adding salt lowers the electrostatic osmotic pressure, leading to the surprising result of a less fuzzy outer surface, and a more fuzzy interior cavity wall. This is due to the expansion of the polymer towards the interior, whereas the outer surface becomes less stretched. Wypysek et al. thus evidence new ways of controlling multi-compartment microgel morphology, by either using T-sensitivity, or charge screening.

Once the core-shell and potentially hollow architectures are well mastered, electrostatic charges can be employed to trigger uptake, storage, and release of polyelectrolyte as generic guest molecules. Naturally, other host-guest interactions may be chosen, like hydrophobicity, but then the convenient pH-trigger of electrostatics to control uptake, storage, and in particular release is usually

lost. Gelissen et al. have studied the introduction of poly(styrene)-sulfonate of various masses into core-shell microgels designed with a cationic polymeric core to attract functional guest molecules [39]. Monomethylitaconate is copolymerized in order to introduce the positive charges. As cationic macromolecules exhibit cell toxicity due to interactions with negatively charged biomolecules, the authors have added an anionic APMH-shell, thus limiting toxicity. This has also the advantage of accumulating the guest molecules inside the particles, avoiding layer formation on the surface which could limit uptake. On the other hand, the total amount of incorporated guest molecules does not seem to be decreased by the presence of the shell, but mostly controlled by the mass of the guest polyelectrolyte: smaller molecules are found to penetrate deeply in the core, while the longer ones remain in the periphery of the core. The latter provide a larger uptake, and due to the reduced interaction with the cationic polyelectrolytes, a more complete release. The corresponding internal microstructure has been shown by detailed SANS modeling based again on the fuzzy core-shell structure of all hydrogenated material – microgel and polyelectrolyte. The characteristic increase of the overall density profile above the value of the pure microgel indicates the presence of the guest molecules. If one excludes reorganization of the microgel morphology itself – this is one of the structural assumptions needed in absence of deuteration as mentioned above –, the effect of density added by chains is clearly seen in Figure 1.10, where the pure microgel volume fraction has been set to one in the center. Its increase shows thus the presence of the polyelectrolyte, which has different locations for short and long chains. As a result, uptake can be performed at low pH where the shell is neutral, and release at high pH. The latter seems to be more efficient for the longer chains, presumably because of their accumulation at the

interface between the two shells. And finally, as often done by these groups, experiments are compared to computer simulations for structure and release kinetics, providing further insight into the mechanisms.

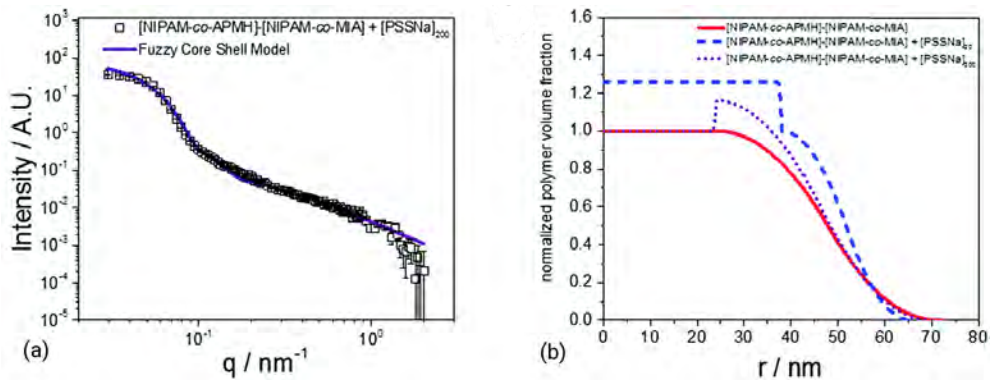

Figure 1.10: (a) Polyampholyte microgel with $[PSSNa]_{200}$ at pH 2 and I = 50 mM. SANS form factor and corresponding fit with a fuzzy coreshell model. (b) Radial profiles as a function of the microgel radius as obtained from fits in (a) for the polyampholyte microgel (solid line), polyampholyte microgel with $[PSSNa]_{20}$ (dashed line) and polyampholyte microgel with $[PSSNa]_{200}$ (dotted line). Note that the volume fraction has been normalized to one in the center of the bare microgel. Reproduced with permission of the Royal Society of Chemistry from ref. [39].

In a French-German collaboration, our own groups have recently revisited the structure of core-shell microgels where the core and the shell monomers, pNIPMAM and pNNPAM, respectively, have different volume transition temperatures, namely ca. 45 ^{o}C and 23 ^{o}C, respectively. This leads to a peculiar swelling behavior as measured by dynamic light scattering, which reports the hydrodynamic radius as a function of temperature [123]. In spite of showing a jump in size at each transition temperature, a linear swelling domain is found between the two transition temperatures. This was first explained by the above-mentioned corset effect [123], where the swelling of the core as the

temperature is lowered from 55^{o}C is hindered by the still collapsed shell of pNNPAM. However, the complete picture is a bit different, as we could show by introducing deuteration of one of the monomers, pNNPAM. Deuteration gives access to the individual spatial distribution of each monomer, the quantitative determination of which is particularly well-performed using the form-free Monte Carlo simulations outlined in the neutron section above, and which will be applied here. In this context, it is worth mentioning that there has been some effort invested into characterizing the consequences of deuteration on the phases. Cors et al. have studied the volume transitions for different deuteration schemes by dynamic light scattering [24]. Among the surprising results, it was shown that the transition temperature is not a monotonous function of the fraction of H-D- replacement. Brugnoni et al. arrived at a similar conclusion in their studies of ultra-low cross-linked pNIPAM microgels, i.e. with synthesis without dedicated cross-linking molecules [17]. They found that the amplitude of the temperature shift depends on the specific group which is substituted, vinyl or isopropyl, only the latter one showing a strong impact of deuteration. Moreover, (self-)cross-linking was also found to be sensitive to, and possibly hindered by deuteration, as found with a deuterated isopropyl group, which presumably is the group responsible for spontaneous cross-linking.

Coming back to the pNIPMAM-core/pNNPAM-shell system, we have first compared the qualitatively new linear swelling behavior in bulk (by PCS) to the one observed for microgel particles adsorbed onto a surface (by ellipsometry), and found that the swelling is robust, i.e. not affected by the surface [21]. In Figure 1.11, this is seen to be robust for different core cross-linking ratios (BIS).

Using the form-free reverse Monte Carlo simulation, we have then solved

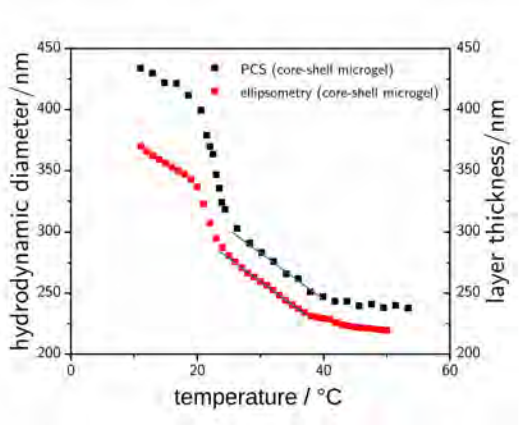

Figure 1.11: Comparison of the swelling of microgel particles in the bulk (in terms of R_h as measured by PCS, scale on the left, black symbols) to the same particles adsorbed on a surface (in terms of layer-thickness as measured by ellipsometry, scale on the right, red symbols). The linear swelling domain is indicated by the blueish lines. Both lines have the same slope. Adapted with permission from [21]. Copyright 2017 American Chemical Society.

the multi-shell model for the pNIPMAM cores, called core-only microgel particles [22]. The resulting volume fraction profile has already been shown in Figure 1.7. The decrease in temperature is seen to cause the swelling of the particle, with a decrease of its density in the core region, which extends to progressively higher radii. At 15 ^{o}C, the fully swollen state is characterized by an approximately constant central zone, which is surrounded by a more and more dilute corona. This core-corona structure is the natural result of the gradient in cross-linker, and not the core-shell structure purpose-synthesized successively with two different monomers, both cross-linked.

The microstructure of the core-shell microgels has also been studied by SANS, in separate experiments made with the same microgel particles, while adapting the solvent [23]. Using a H_2O/D_2O solvent rich in light water allows matching the hydrogenated monomers (pNIPMAM), and the inverse is true

for the pNNPAM shell. The scattered intensity thus reflects only the spatial distribution of the non-matched component. In Figure 1.12, the density profile of the core monomers within the core- shell microgel is plotted, for invisible but present shell monomers. While the set of curves follows mostly the same sequence as the core-only particles already shown in Figure 1.7, the surprising result is that the density of the core-monomers has not been increased by the surrounding deuterated pNNPAM shell, but actually decreased. This stands at odds with our own (naive) interpretation of the corset effect, which states that the shell actually compresses the core, and should therefore increase its density.

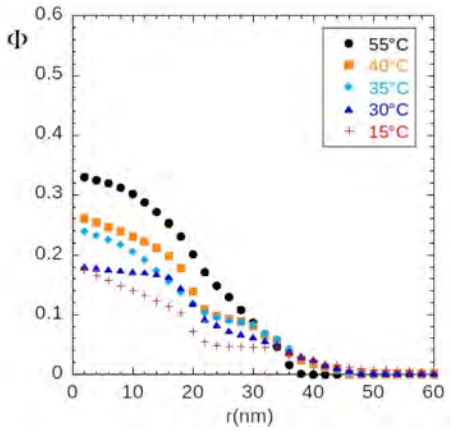

Figure 1.12: Density profile of the core monomers of the H-pNIPMAM-core D7-pNNPAM-shell system with the same core as in Fig. 1.7, and a contrast matched shell (CCC = 1.9 mol%). Adapted with permission from [24].

The complementary SANS measurements of the pNIPMAM-pNNPAM microgels with a deuterated shell monomer in mostly hydrogenated solvent matching the pNIPMAM has provided molecular understanding of the above surprise: the now visible shell monomers do not form a homogeneous shell around the

core, but rather penetrate into it down to the center of the microgel particle. In Figure 1.13a, the scattered intensities for different temperatures are found to be well described by the model. The corresponding shell monomer density profiles are reproduced in Figure 1.13. As a surprising result of monomer compatibility at high temperatures, the so-called shell monomer is actually more abundant in the core than the core monomers themselves! It looks like the second polymerization fills up the holes and meshes, before finishing its polymerization with a thin shell around the composite core. Obviously, this result must be system-dependent, because higher amounts of shell monomer would then induce the growth of a true shell. In the present case, however, the result is a monomer concentration gradient throughout the microgel, which presumably leads to different transition temperatures for each piece of material, depending on its distance from the center. This progressive evolution of the transition temperature is probably responsible for the striking linear swelling behavior shown in Figure 1.11.

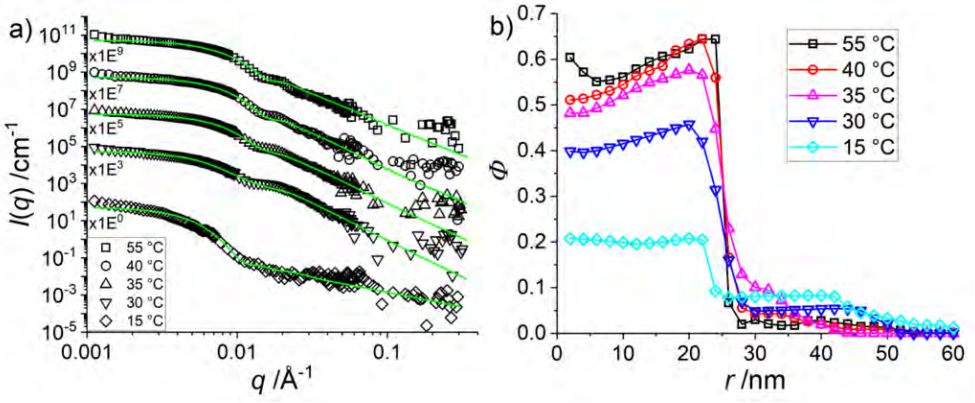

Figure 1.13: H-pNIPMAM core with D7-pNNPAM shell with a CCC of 10 mol% (a): $I(q)$ vs. q of SANS measurements with a H_2O/D_2O that matches the core. (b): Calculated monomer density profile of the pNNPAM shell from the SANS data in a). Reproduced with permission of the Royal Society of Chemistry from ref. [25].

1.4. Time-resolved small-angle scattering

According to Tanaka and Filmore [111] the swelling kinetics of gels scales with their largest dimension. Macroscopic gels are therefore rather slow in reaching their equilibrium state which limits their usefulness in sensor or actuator design. However, since the smallest dimension is decisive for the kinetics, microgels can have very short response times. A good way to measure the response time of colloidal gels is the use of classical relaxation methods like p- or T-jump and stopped flow techniques combined with fast scattering methods to follow the induced structural changes. The stopped flow technique was successfully used by the Richtering group in the study of de-swelling of microgels triggered by mixing the aqueous microgel solution with alcohol. In this experiment, the co-nonsolvency effect is exploited to induce the volume transition of the particles in the mixing cuvette [56]. The experiments were done at the European Synchrotron Radiation Facility (ESRF) (Grenoble, France) using the ID02 SAXS beamline. The stopped-flow system was employed for ultrafast mixing of a microgel solution in pure methanol and a methanol water mixture with $\mathrm{X}_{MeOH} \approx 0.2$.

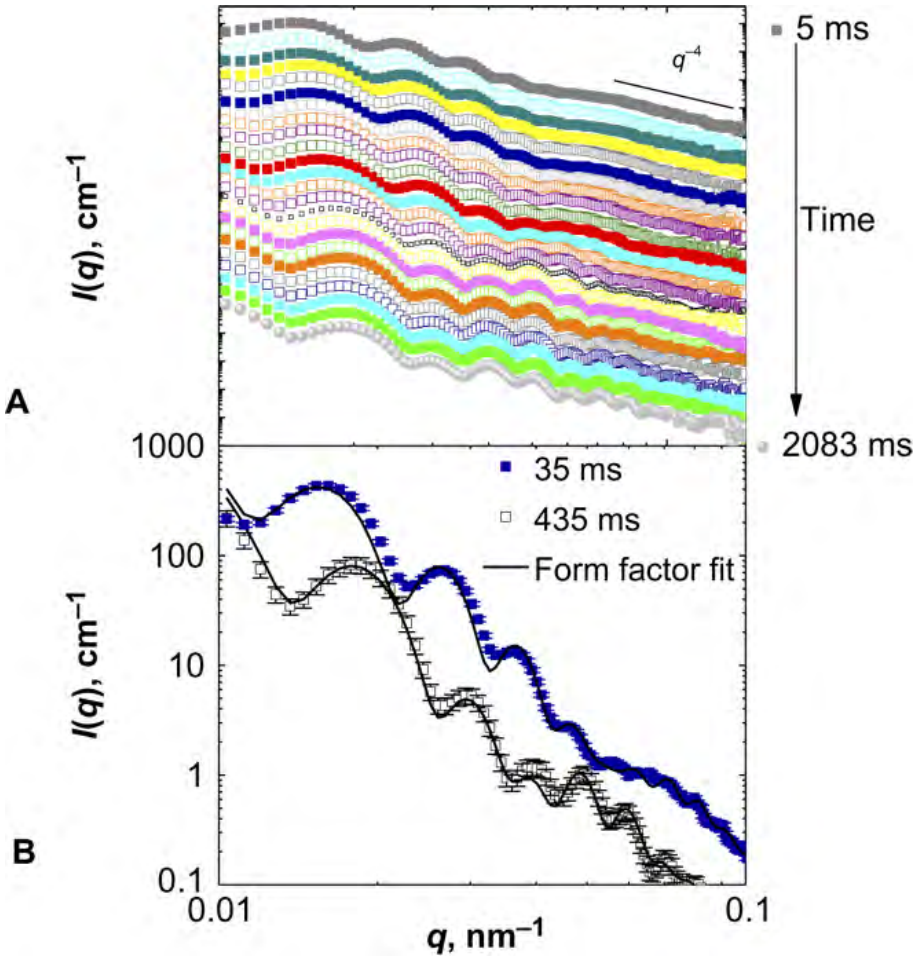

Figure 1.14: (A) SAXS patterns of PNIPAM microgels for the solvent composition change from pure MeOH to $X_{MeOH} \approx 0.2$ at different times. (B) Examples of form factor fits for two SAXS patterns obtained at 35 and 435 ms after mixing (for better visibility, the intensity of the SAXS pattern at 435 ms is shifted vertically by a factor of 0.3). Reproduced with permission from ref. [56].

In Fig. 1.14A the SAXS data are plotted as a function of time. The statistics of the SAXS data is sufficiently good to allow a fit with a form factor model. In combination with simulations, the authors have shown that the collapse is a two-step process with two largely different time constants of $\tau_1 = 1.3$ ms

and $\tau_2 = 2227$ ms. These results are in good agreement with recent stroboscopic p-jump SANS experiments by Wrede et al. [120]. The experiments were performed on the D11 small-angle scattering machine at the Institute Laue Langevin which has a time-resolution of 2ms. The authors used a home built pressure jump device allowing also 2ms of dead-time. However, in contrast to the work by the Richtering group, here a poly(N-n-PAM) microgel was studied. Also in this case two relaxation times were observed for the pressure induced collapse. Swelling is characterized by only one relaxation time.

Also the growth kinetics of microgels can be studied by time-resolved scattering techniques. The synthesis of nano- and microgels is usually done using bad solvent conditions for the respective polymer which is employed. After initiation, the forming oligomers phase separate and form a nucleus for the further precipitation of growing chains. However, many details of this so-called precipitation polymerization are still unknown. Here, time-resolved scattering experiments are of paramount importance to achieve a more detailed understanding of the process. An interesting example for such a study is the article by Virtanen and co-workers [116]. These authors investigated several initial conditions with respect to their influence on the formation of standard PNIPAM microgels.

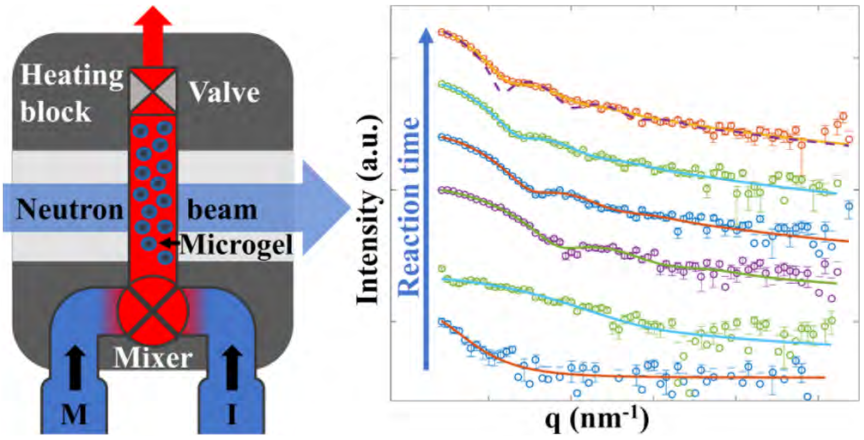

Figure 1.15: Scheme of the setup used by Virtanen et al. (left) and some examples for the measured form factors (right). Already by bare eye one can observe the increasing particle size. Reproduced with permission from https://pubs.acs.org/doi/10.1021/acsomega.8b03461.

Virtanen et al. have performed their experiments at the Heinz Maier-Leibnitz Zentrum (MLZ) (Munich, Germany) using the KWS-2 SANS machine. They used a stopped-flow device with the sample cell mounted in a heating block (see Fig. 1.15 left). Heat is used to initiate the reaction after rapid mixing. The use of such a device allows repeating the time-resolved recording of the scattering data until sufficiently good data statistics is obtained by summing up time binned data of several shots. This approach was introduced by Isabelle Grillo [6] and has been used for the study of structural changes in a number of colloidal systems. The right-hand-side of Fig. 1.15 shows typical SANS scattering curves as obtained at different times in the course of the reaction. Already a qualitative look at the curves shows that the particles are indeed growing. An example for the obtained kinetic curves is shown in Fig. 1.16.

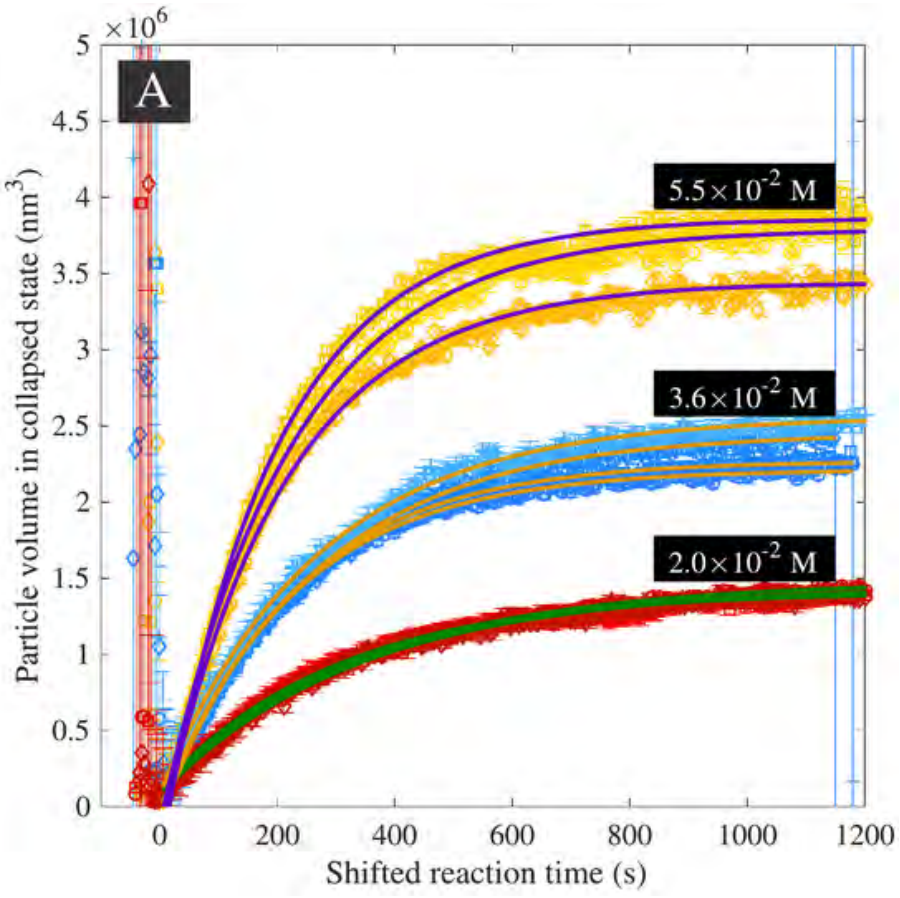

Figure 1.16: Series of kinetic data obtained for different initial PNIPAM concentrations. Reproduced with permission from https://pubs.acs.org/doi/10.1021/acsomega.8b03461.

The polymerization rate is determined by the concentration and transport of the unreacted monomer, since the initiator concentration is nearly constant during the course of the reaction. Due to this the mean particle volume is growing according to a pseudo-first order kinetics. Virtanen et al. have confirmed this by calorimetric measurements of the polymerization process. Moreover, also the influence of the initiator and the cross-linker were studied in this work. The particle number density in the reaction volume is found to decrease due to

peroxide initiator-induced self-crosslinking of NIPAM. The same phenomenon occurs upon increasing the amount of cross-linker. The most important outcome is related to the finding that a certain number of nuclei is created during the early stages of the reaction. Afterwards the number density is found to stay constant. This explains the very low polydispersity usually achieved in a precipitation polymerization.

1.5. Crowded microgel systems

Up to here we have reported on microgel particles in dilute suspension, without interaction between neighboring particles possibly modifying their swelling behavior and morphology. The two main types of interaction are steric potentials which impede corona overlap, and electrostatics, which is caused by the ionic comonomers as already explored above. For low ionic strengths, electrostatic repulsion may have a range such that such interactions play a role. In this case, it is the ratio between Debye length and average inter-particle distance which determines if the regime is indeed dilute, or not. In any case, increasing the particle number density inevitably introduces interactions, which may thus be of electrostatic or steric origin, including soft-core repulsion. Several groups have focused on the morphology and swelling behavior of microgel particles embedded in a sea of other particles, or surrounded by other molecules, and some recent work is reviewed below.

As this chapter focuses mainly on small-angle scattering experiments, a key difference between SAXS and SANS should be emphasized here. In SAXS, it is complicated to modify particle contrast, although some possibilities using anomalous X-ray scattering exist [3] or in some cases the electron density of

the solvent can be changed by sugar addition [38, 27]. However, the sugar moelcules drastically change the solvent properties and might also influence the particle interaction potential in an unwanted way.

In concentrated microgel systems, the interferences of waves scattered by different particles thus overlap with the self-scattering, i.e. the form factor, averaged over all particles [67]. The more concentrated the suspension, the stronger the perturbation of the form factor – which contains the morphological information – by the structure factor encoding the inter-particle correlations. On the contrary, SANS is very sensitive to deuteration, and synthesis of the same type of microgel particle, i.e. same size, monomer, and densities, in two versions, one deuterated, one hydrogenated, is a feasible task. Naturally, some minor discrepancies may remain due to polymerization issues, but also because hydrogenated and deuterated molecules do not have exactly identical physical properties. Nonetheless, it is often possible to either contrast match one of the two species via the solvent mixture, and thereby reduce the effective density of the visible species, or, even better, perform a zero-average contrast experiment [26, 5]. In the latter case, the structure factor cancels due to some "magic" compensation of interferences between H-D and H-H and D-D particles. The latter method needs to be carefully designed when preparing experiments, but turns out to be extremely powerful for the analysis of concentrated suspensions.

The work by Nöjd et al. perfectly illustrates the usefulness of SAXS and SANS, respectively [76]. These authors have studied pNIPAM microgels copolymerized with acrylic acid. Before mixing fully deuterated and fully hydrogenated particles in water, dilute and partially charged microgels at low pH were compared by PCS, finding that they were close in size, of similar swelling

properties, and only slightly shifted in transition temperature (see discussion of refs. [23] and [18] in section 1.3). In the following concentration series, both particles were mixed with H_2O/D_2O in the appropriate ratio in order to fulfill the zero-average contrast condition. In Figure 1.17A, the SANS intensities have been plotted, and they are seen to have no influence of structure factors, i.e. the matching worked perfectly. In Figure 1.17B, the same samples have been measured with SAXS. Here, the deuteration does not modify the electron-density distribution. Thus the full intensity with form and structure is obtained. Very prominent structure factor peaks arise, which have been described by the authors by a variant of a well-known solution of integral equations called renormalized mean spherical approximation. The original form of the latter takes electrostatic interactions into account, and its modification by penetrating solvent typical for hydrogels. In both SAXS and SANS, the form factor can be described by a fuzzy sphere plus polymer network fluctuations. Intensity measurements in absolute values then provide a mass determination of the particles, using eq. 1.11. At the lowest concentrations, the measurements are complemented by static and dynamic light scattering, both highlighting persistent interactions. To summarize, the authors report that these ionic microgels are quite swollen at close to infinite dilution due to electrostatic forces coming from partial protonation of acrylic acid. Via solution of a Poisson-Boltzmann cell model for the core, and Monte Carlo simulations of the dangling-ends forming the corona, they highlight the electrostatic effect on the particle structure, termed porcupine in a zoological analogy. At intermediate concentrations, the microgels decrease in size, and reach an almost constant core radius throughout the SANS regime. Only at the highest concentrations, when the effective volume fraction approaches one, a weak shrinking is ob-

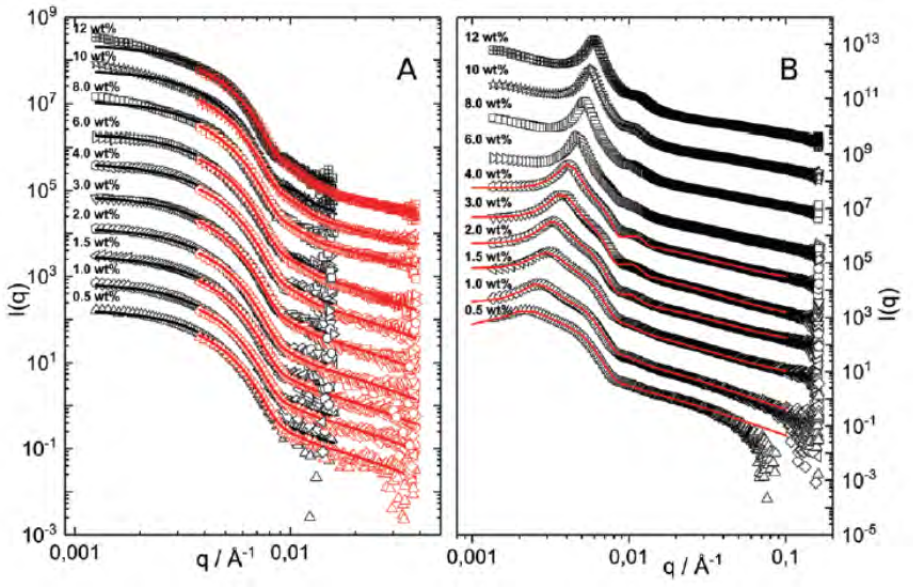

Figure 1.17: (A) SANS data obtained as a function of concentration as indicated in the legend. Solid lines are fits to the data using the fuzzy sphere model. (B) SAXS data obtained using the same samples as in A. The solid lines are fits to the data based on input information from A taking the structure factor into account. All curves are offset along the ordinate for clarity. Reproduced from Ref. [76] with permission of the Royal Society of Chemistry.

served.

In a follow-up, the same group has studied H- and D-microgels in presence of alternating electric fields, also under zero-average contrast [77]. The fuzzy sphere model successfully describes particle shapes for high and low fields, indicating that particles are not deformed by external electric forces. They are, however, found to align, as evidenced by laser scanning confocal microscopy. The SANS measurements thus allow to show that in spite of the decrease of interparticle distances in the strings, there is no particle compression or deformation, but apparently only particle interpenetration. The latter is probably the mechanism responsible for long-lived metastable crystalline states, which

have to overcome chain entanglement between microgel particles in order to rearrange.

However, in recent work by Scotti [101] the conclusion is slightly different which is probably related to the fact that in the works by Nöjd et al. only linearly aligned particles were studied. Determination of the real volume fraction of microgels is not at all trivial and the chemical composition has a major influence on possible particle deformation. Scotti has addressed this problem also using contrast variation having partly deuterated microgels as a matrix for nearly identical hydrogenated particles. Using appropriate heavy and light water mixtures allows to measure an apparent form factor for dilute hydrogenated microgels which are nevertheless compressed by the matrix. For NIPAM microgels with 5 mol% cross-linker he has observed that up to a volume fraction of 0.64 no significant deviation between the real and the so-called generalized volume fraction occurs. Beyond this value the real volume fraction is smaller than the generalized volume fraction based on the radius of the diluted particles. Hence, at $\phi = 0.64$ for these microgels compression sets in. For ultralow cross-linked microgels compression starts even earlier at $\phi = 0.58$. The compression of microgels was found to lead to faceting [20] using super-resolution optical microscopy. In his work Scotti uses this phenomenon to explain the observed increase in apparent polydispersity in the form factor fits.

As with monodisperse hard spheres, microgel particles may crystallize at high concentrations. As soon as polydispersity exceeds some 12% for hard spheres, crystallization is suppressed. But contrary to hard spheres, microgels may also adapt their shape, and possibly size. Scotti et al. have followed this idea by comparing phase diagrams and scattering of microgel mixtures of controlled polydispersity, comparing in particular Gaussian polydispersity to bidispersity

with a ratio in size of 1.3 to 1.4 [98]. They focus on a concentration study of the fully swollen state of pNIPAM accessible at room temperature. By introducing bidispersity, the size mismatch impedes in theory crystallization. Due to the presence of electrostatic charges caused by the initiator molecules, the counter ion pressure is sensitive to the microgel concentration, and responsible for shrinking at high concentrations [102]. By analyzing the apparent structure factors relying on polydisperse fuzzy sphere form factors measured at high dilution – it has been checked independently that this introduces only little error in peak shape and position –, this study finds that the bigger microgel particles shrink preferentially, thus reducing the polydispersity. The resulting S(q) resembles the one of the small particles only, indicating that the bigger ones have deswollen, thus favoring crystallization up to a number fraction of ca. 30% of big particles. Concerning Gaussian polydispersity, the flexibility of the microgel allows accommodating up to almost 20% polydispersity and still crystallize, presumably due to the shrinking of the large-size tail of the distribution.

The next step taken in concentration studies was to introduce a new degree of freedom, by taking advantage of the hollow microgels discussed in section 1.3. The presence of the cavity naturally allows the microgel particles to adjust to external pressure exerted by the surrounding microgels, which have been chosen to be plain but of identical cross-linking and (almost identical) hydrodynamic radius. The group takes nicely advantage of the properties of neutron scattering, by contrast matching via the solvent mixture of light and heavy water the plain microgel particle, and highlighting thus only the hollow ones [99]. As their concentration was deliberately kept low, the structure factor influence becomes negligible, and they measure directly the form factor, which has been described by the usual fuzzy hollow-shell model. It may be noted

that the form-free model (see section 1.2) has been applied as a cross-check, and provides virtually identical profiles. As a result, the cavity is seen to be preserved up to moderate volume fraction. At higher pressures, the polymer extends into the cavity, and simultaneously the outer fuzziness of the hollow microgels disappears.

In a subsequent step, Scotti et al. comparatively discuss the influence of microgel cross-linking and architecture on morphology under pressure at high concentrations [103]. They use the same contrast matching approach of the matrix of microgels exerting the pressure on some selected, non deuterated microgels. They confirm the important role of the cavity, which in particular has a stronger contribution to deswelling than the decrease of the cross-link density by a factor of two.

As a final point in this review of recent work on concentrated microgels, we propose to highlight a completely different approach. The effect of increase in concentration of microgel particles is usually studied in a molecular solvent, as in the above studies. An interesting crossover has been proposed by Schneider et al., who study the effect of added linear polymer chains replacing the solvent [95]. Their microgel particles are made of p(N-polyvinylcaprolactam), of swollen size in heavy water about 200 nm. These particles are incorporated in PEG melts of different chain mass using a common solvent and subsequent evaporation. With dPEG, the microgel particles gain neutron visibility, and bumps in the SANS intensity can be described by a core-shell model with fuzziness. Surprisingly, the small polymer chains gain also visibility, indicating a molecular mixture, i.e. interpenetration into the microgels, for the smallest masses of below 3k. The larger masses do not show chain scattering if samples are fully equilibrated, and a strong low-q increase seems to indicate phase sepa-

ration. At high temperatures, between 160 and 180^{o}C, the microgels are found to deswell, they thus seem to cross a critical temperature interpreted as LCST. This results in the expulsion of matrix chain molecules, with a corresponding decrease of the visibility of the latter. If this happens at high microgel concentrations, the particles appear to order in the majority phase in close contact, and the corresponding peak position shifts with the deswelling.

1.6. Conclusion and outlook

Micro- and nanogels are a very active research topic, and we have given a necessarily subjective view of recent progress in the field. Our focus was directed towards new particle morphologies, but also included evolution of particle structure with external stimuli including solvent, pressure, and temperature jumps, as well as internal stimuli like the pressure exerted by neighboring particles. For such studies, the use of scattering techniques is crucial, due to their non destructive and possibly time-resolved measurements of both particle architectures and interactions. In particular neutron scattering is a very powerful method, as (partial) deuteration can be used to localize different monomers and particles in space via isotopic substitution, zero-average contrast, and in general contrast variation methods. Given the importance of these methods, we have also provided an overview of the analysis of static and dynamic scattering data. In particular density profile approaches have provided deep insight into particle morphologies. With an admittedly scholarly presentation of both the underlying mechanisms, and some "hands-on" tools on how to access the relevant information, we hope to have convinced the reader that scattering is a highly suitable tool for microgel studies.

It is noteworthy that only very few systems were characterized with respect to growth kinetics. Especially for copolymer systems at least to our knowledge no data are available, and we hope that new experiments with ever more powerful instruments will allow unraveling the details of such mostly unknown processes. We are looking forward to reading such results in the literature, and hope that our modest contribution here will be useful for scientists working in the field.

Appendix: Absolute intensity for fuzzy sphere form factors

The expression in eq. 1.5 is the product of the normalized hard sphere form factor by a Gaussian. This product in q-space corresponds to a convolution in r-space by a Gaussian, and as the Gaussian is symmetric, the weighting by the volume is usually overlooked in the literature. This leads to absolute intensity predictions with slight errors, of the order of 10% depending on fuzziness. In other words, the integral over the profile describing the density function contains a term $4\pi r^2$, which is asymmetric around the nominal radius $r = R$, and increases the weighting of the outer zones of higher r. It is straightforward to calculate that in the case of a 10% interfacial width ($\frac{\sigma}{R} = 10\%$), the correction factor is 1.03, and for 20%, it is ca. 1.12. The effect of fuzziness is to increase the particle size visible in the Guinier regime, and this should be accompanied by the above intensity correction, although it is usually not explicitly included in form factor equations like eq. 1.5.

Moreover, the enveloping high-q power law is shifted to a slope steeper than the Porod law, thereby decreasing the higher-order form factor oscillations, as expected for fuzziness.

Bibliography

[1] Marco Annegarn, Maxim Dirksen, and Thomas Hellweg. Importance of pH in synthesis of pH-responsive cationic nano- and microgels. *Polymers*, 13(5):827, mar 2021. doi: 10.3390/polym13050827.

[2] Andreea Balaceanu, Veronica Mayorga, Wanjuan Lin, Marco-Philipp Schürings, Dan E. Demco, Alexander Böker, Mitchell A. Winnik, and Andrij Pich. Copolymer microgels by precipitation polymerisation of n-vinylcaprolactam and n-isopropylacrylamides in aqueous medium. *Colloid and Polymer Science*, 291(1):21–31, may 2012. doi: 10.1007/s00396-012-2659-1.

[3] M. Ballauff. SAXS and SANS studies of polymer colloids. *Current Opinion in Colloid & Interface Science*, 6(2):132–139, may 2001. doi: 10.1016/s1359-0294(01)00072-3.

[4] Matthias Ballauff and Yan Lu. "Smart" nanoparticles: Preparation, characterization and applications. *Polymer*, 48(7):1815–1823, mar 2007. doi: 10.1016/j.polymer.2007.02.004.

[5] Amélie Banc, Anne-Caroline Genix, Christelle Dupas, Michael Sztucki, Ralf Schweins, Marie-Sousai Appavou, and Julian Oberdisse. Origin of small-angle scattering from contrast-matched nanoparticles: A study of

chain and filler structure in polymer nanocomposites. *Macromolecules*, 48(18):6596–6605, sep 2015. doi: 10.1021/acs.macromol.5b01424.

[6] A. Barth, I. Grillo, and M. Gradzielski. Dynamics of formation of vesicles studied by highly time-resolved stopped-flow experiments. *Tenside Surfactants Detergents*, 47(5):300–306, sep 2010. doi: 10.3139/113.110081.

[7] D.J. Bell, S. Ludwanowski, A. Lüken, B. Sarikaya, A. Walther, and M. Wessling. Hydrogel membranes made from crosslinked microgel multilayers with tunable density. *Journal of Membrane Science*, 620:118912, feb 2021. doi: 10.1016/j.memsci.2020.118912.

[8] Maxime J. Bergman, Jan S. Pedersen, Peter Schurtenberger, and Niels Boon. Controlling the morphology of microgels by ionic stimuli. *Soft Matter*, 16(11):2786–2794, 2020. doi: 10.1039/c9sm02170a.

[9] Ingo Berndt, Jan Skov Pedersen, Peter Lindner, and Walter Richtering. Influence of shell thickness and cross-link density on the structure of temperature-sensitive poly-*N*-isopropylacrylamide-poly-n-isopropylmethacrylamide core-shell microgels investigated by small-angle neutron scattering. *Langmuir*, 22(1):459–468, jan 2006. doi: 10.1021/la052463u.

[10] Bruce J. Berne and Robert Pecora. *Dynamic Light Scattering: With Applications to Chemistry, Biology, and Physics*. Dover Publications Inc., 2000. ISBN 978-0486411552. URL https://www.ebook.de/de/product/3344676/bruce_j_berne_robert_pecora_physics_dynamic_light_scattering_with_applications_to_chemistry_biology_and_physics.html.

[11] Daniel Besold, Sebastian Risse, Yan Lu, Joachim Dzubiella, and Matthias

Ballauff. Kinetics of the reduction of 4-nitrophenol by silver nanoparticles immobilized in thermoresponsive core–shell nanoreactors. *Industrial & Engineering Chemistry Research*, 60(10):3922–3935, mar 2021. doi: 10.1021/acs.iecr.0c06158.

[12] William H. Blackburn, Erin B. Dickerson, Michael H. Smith, John F. McDonald, and L. Andrew Lyon. Peptide-functionalized nanogels for targeted sirna delivery. *Bioconjugate chemistry*, 20(5):960–968, 2009. doi: 10.1021/bc800547c.

[13] Johannes Bookhold, Maxim Dirksen, Lars Wiehemeier, Sebastian Knust, Dario Anselmetti, Florian Paneff, Xianghui Zhang, Armin Gölzhäuser, Tilman Kottke, and Thomas Hellweg. Smart membranes by electron beam cross-linking of copolymer microgels. *Soft Matter*, 17(8):2205–2214, 2021. doi: 10.1039/d0sm02041a.

[14] Niels Boon and Peter Schurtenberger. Swelling of micro-hydrogels with a crosslinker gradient. *Physical Chemistry Chemical Physics*, 19(35): 23740–23746, 2017. doi: 10.1039/c7cp02434g.

[15] Robert Botet, Sylvie Kwok, and Bernard Cabane. Percus–Yevick structure factors made simple. *Journal of Applied Crystallography*, 53(6): 1570–1582, nov 2020. doi: 10.1107/s1600576720014041.

[16] Monia Brugnoni, Andrea Scotti, Andrey A. Rudov, Arjan P. H. Gelissen, Tobias Caumanns, Aurel Radulescu, Thomas Eckert, Andrij Pich, Igor I. Potemkin, and Walter Richtering. Swelling of a responsive network within different constraints in multi-thermosensitive microgels. *Macromolecules*, 51(7):2662–2671, mar 2018. doi: 10.1021/acs.macromol.7b02722.

[17] Monia Brugnoni, Anne C. Nickel, Leif C. Krger, Andrea Scotti, Andrij Pich, Kai Leonhard, and Walter Richtering. Synthesis and structure of deuterated ultra-low cross-linked poly(N-isopropylacrylamide) microgels. *Polymer Chemistry*, 10(19):2397–2405, 2019. doi: 10.1039/c8py01699b.

[18] Monia Brugnoni, Fabian Fink, Andrea Scotti, and Walter Richtering. Synthesis and structure of temperature-sensitive nanocapsules. *Colloid and Polymer Science*, 298(9):1179–1185, jun 2020. doi: 10.1007/s00396-020-04686-5.

[19] Kimberly C. Clarke, Simon N. Dunham, and L. Andrew Lyon. Core/shell microgels decouple the pH and temperature responsivities of microgel films. *Chemistry of Materials*, 27(4):1391–1396, feb 2015. doi: 10.1021/cm504649t.

[20] Gaurasundar M. Conley, Philippe Aebischer, Sofi Njd, Peter Schurtenberger, and Frank Scheffold. Jamming and overpacking fuzzy microgels: Deformation, interpenetration, and compression. *Science Advances*, 3 (10):e1700969, oct 2017. doi: 10.1126/sciadv.1700969.

[21] Marian Cors, Oliver Wrede, Anne-Caroline Genix, Dario Anselmetti, Julian Oberdisse, and Thomas Hellweg. Core–shell microgel-based surface coatings with linear thermoresponse. *Langmuir*, 33(27):6804–6811, jun 2017. doi: 10.1021/acs.langmuir.7b01199.

[22] Marian Cors, Lars Wiehemeier, Yvonne Hertle, Artem Feoktystov, Fabrice Cousin, Thomas Hellweg, and Julian Oberdisse. Determination of internal density profiles of smart acrylamide-based microgels by small-angle neutron scattering: A multishell reverse monte carlo approach.

Langmuir, 34(50):15403–15415, nov 2018. doi: 10.1021/acs.langmuir.8b03217.

[23] Marian Cors, Lars Wiehemeier, Julian Oberdisse, and Thomas Hellweg. Deuteration-induced volume phase transition temperature shift of PNIPMAM microgels. *Polymers*, 11(4):620, apr 2019. doi: 10.3390/polym11040620.

[24] Marian Cors, Oliver Wrede, Lars Wiehemeier, Artem Feoktystov, Fabrice Cousin, Thomas Hellweg, and Julian Oberdisse. Spatial distribution of core monomers in acrylamide-based core-shell microgels with linear swelling behaviour. *Scientific Reports*, 9(1), sep 2019. doi: 10.1038/s41598-019-50164-6.

[25] Marian Cors, Lars Wiehemeier, Oliver Wrede, Artem Feoktystov, Fabrice Cousin, Thomas Hellweg, and Julian Oberdisse. Contrast variation SANS measurement of shell monomer density profiles of smart core–shell microgels. *Soft Matter*, 16(7):1922–1930, 2020. doi: 10.1039/c9sm02036e.

[26] J.P. Cotton. Variations on contrast in SANS: determination of self and distinct correlation functions. *Advances in Colloid and Interface Science*, 69(1-3):1–29, dec 1996. doi: 10.1016/s0001-8686(96)00306-5.

[27] Carina Dargel, Yvonne Hannappel, and Thomas Hellweg. Heating-induced DMPC/glycyrrhizin bicelle-to-vesicle transition: A x-ray contrast variation study. *Biophysical Journal*, 118(10):2411–2425, may 2020. doi: 10.1016/j.bpj.2020.03.022.

[28] Mallika Das, Nicolas Sanson, Daniele Fava, and Eugenia Kumacheva. Microgels loaded with gold nanorods: photothermally triggered volume

transitions under physiological conditions. *Langmuir*, 23(1):196–201, jan 2007. doi: 10.1021/la061596s.

[29] Justin D. Debord and L. Andrew Lyon. Thermoresponsive photonic crystals. *The Journal of Physical Chemistry B*, 104(27):6327–6331, jul 2000. doi: 10.1021/jp001238c.

[30] P. Debye. Molecular-weight determination by light scattering. *The Journal of Physical and Colloid Chemistry*, 51(1):18–32, jan 1947. doi: 10.1021/j150451a002.

[31] Laura Etchenausia, Elise Deniau, Annie Brûlet, Jacqueline Forcada, and Maud Save. Cationic thermoresponsive poly(n-vinylcaprolactam) microgels synthesized by emulsion polymerization using a reactive cationic macro-RAFT agent. *Macromolecules*, 51(7):2551–2563, mar 2018. doi: 10.1021/acs.macromol.8b00155.

[32] A. Fernández-Nieves, A. Fernández-Barbero, B. Vincent, and F. J. de las Nieves. Charge controlled swelling of microgel particles. *Macromolecules*, 33(6):2114–2118, mar 2000. doi: 10.1021/ma991520l.

[33] Paul J. Flory and John Rehner. Effect of deformation on the swelling capacity of rubber. *The Journal of Chemical Physics*, 12(10):412–414, oct 1944. doi: 10.1063/1.1723884.

[34] S Franco, E Buratti, B Ruzicka, V Nigro, N Zoratto, P Matricardi, E Zaccarelli, and R Angelini. Volume fraction determination of microgel composed of interpenetrating polymer networks of PNIPAM and polyacrylic acid. *Journal of Physics: Condensed Matter*, 33(17):174004, apr 2021. doi: 10.1088/1361-648x/abe1ec.

[35] Krista G. Freeman, Jacob Adamczyk, and Kiril A. Streletzky. Effect of synthesis temperature on size, structure, and volume phase transition of polysaccharide microgels. *Macromolecules*, 53(21):9244–9253, oct 2020. doi: 10.1021/acs.macromol.0c01605.

[36] Lara Frenzel, Felix Lehmkühler, Michael Koof, Irina Lokteva, and Gerhard Grübel. The phase diagram of colloidal silica–PNIPAm core–shell nanogels. *Soft Matter*, 16(2):466–475, 2020. doi: 10.1039/c9sm01884k.

[37] B. J. Frisken. Revisiting the method of cumulants for the analysis of dynamic light-scattering data. *Applied optics*, 40(24):4087–4091, 2001. ISSN 1559-128X. doi: 10.1364/AO.40.004087.

[38] Raul Garcia-Diez, Christian Gollwitzer, Michael Krumrey, and Zoltan Varga. Size determination of a liposomal drug by small-angle x-ray scattering using continuous contrast variation. *Langmuir*, 32(3):772–778, jan 2016. doi: 10.1021/acs.langmuir.5b02261.

[39] Arjan P. H. Gelissen, Andrea Scotti, Sarah K. Turnhoff, Corinna Janssen, Aurel Radulescu, Andrij Pich, Andrey A. Rudov, Igor I. Potemkin, and Walter Richtering. An anionic shell shields a cationic core allowing for uptake and release of polyelectrolytes within core–shell responsive microgels. *Soft Matter*, 14(21):4287–4299, 2018. doi: 10.1039/c8sm00397a.

[40] Tibor Gilányi, Imre Varga, Róbert Meszáros, Genoveva Filipcsei, and Miklós Zrínyi. Characterisation of monodisperse poly(*N*-isopropylacrylamide) microgel particles. *Physical Chemistry Chemical Physics*, 2(9):1973–1977, 2000. doi: 10.1039/b000571l.

[41] O. Glatter. A new method for the evaluation of small-angle scattering data. *J.Appl. Cryst.*, 10:415–421, 1977.

[42] O. Glatter. Data evaluation in small angle scattering: calculation of the radial electron density distribution by means of indirect fourier transformation. *Acta Phys. Austriaca*, 47:83–102, 1977.

[43] Boualem Hammouda. Small-angle scattering from branched polymers. *Macromolecular Theory and Simulations*, 21(6):372–381, mar 2012. doi: 10.1002/mats.201100111.

[44] Yvonne Hannappel, Lars Wiehemeier, Maxim Dirksen, Tilman Kottke, and Thomas Hellweg. Smart microgels from unconventional acrylamides. *Macromolecular Chemistry and Physics*, page 2100067, may 2021. doi: 10.1002/macp.202100067.

[45] Jean-Pierre Hansen and John B. Hayter. A rescaled MSA structure factor for dilute charged colloidal dispersions. *Molecular Physics*, 46(3): 651–656, jun 1982. doi: 10.1080/00268978200101471.

[46] Jean-Pierre Hansen and Ian R. McDonald. *Theory of Simple Liquids*. Elsevier, 2013. doi: 10.1016/c2010-0-66723-x.

[47] Thomas Hellweg. Responsive core-shell microgels: Synthesis, characterization, and possible applications. *Journal of Polymer Science Part B: Polymer Physics*, 51(14):1073–1083, may 2013. doi: 10.1002/polb.23294.

[48] Thomas Hellweg, Karl Kratz, Stephanie Pouget, and Wolfgang Eimer. Internal dynamics in colloidal PNIPAM microgel particles immobilised in mesoscopic crystals. *Colloids and Surfaces A: Physicochemical*

and Engineering Aspects, 202(2-3):223–232, apr 2002. doi: 10.1016/s0927-7757(01)01077-9.

[49] Yvonne Hertle, Michael Zeiser, Christoph Hasenhrl, Peter Busch, and Thomas Hellweg. Responsive p(NIPAM-co-NtBAM) microgels: Flory–Rehner description of the swelling behaviour. *Colloid and Polymer Science*, 288(10-11):1047–1059, may 2010. doi: 10.1007/s00396-010-2232-8.

[50] Todd Hoare and Robert Pelton. Highly pH and temperature responsive microgels functionalized with vinylacetic acid. *Macromolecules*, 37(7): 2544–2550, apr 2004. doi: 10.1021/ma035658m.

[51] John S. Hyatt, Changwoo Do, Xiaobo Hu, Hong Sung Choi, Jin Woong Kim, L. Andrew Lyon, and Alberto Fernandez-Nieves. Segregation of mass at the periphery of$N$-isopropylacrylamide-co-acrylic-acid microgels at high temperatures. *Physical Review E*, 92(3), sep 2015. doi: 10.1103/physreve.92.030302.

[52] John S. Hyatt, Alison M. Douglas, Chris Stanley, Changwoo Do, Thomas H. Barker, and Alberto Fernández-Nieves. Charge segregation in weakly ionized microgels. *Physical Review E*, 95(1), jan 2017. doi: 10.1103/physreve.95.012608.

[53] Molla R. Islam, Chelsey Nguy, Sanika Pandit, and Louis Andrew Lyon. Design and synthesis of core–shell microgels with one-step clickable crosslinked cores and ultralow crosslinked shells. *Macromolecular Chemistry and Physics*, 221(19):2000156, sep 2020. doi: 10.1002/macp.202000156.

[54] Matthias Karg, Andrij Pich, Thomas Hellweg, Todd Hoare, L. Andrew Lyon, J. J. Crassous, Daisuke Suzuki, Rustam A. Gumerov, Stefanie Schneider, Igor I. Potemkin, and Walter Richtering. Nanogels and microgels: From model colloids to applications, recent developments, and future trends. *Langmuir*, 35(19):6231–6255, 2019. ISSN 0743-7463. doi: 10.1021/acs.langmuir.8b04304.

[55] Martina Keerl, Jan Skov Pedersen, and Walter Richtering. Temperature sensitive copolymer microgels with nanophase separated structure. *Journal of the American Chemical Society*, 131(8):3093–3097, feb 2009. doi: 10.1021/ja807367p.

[56] Rico Keidel, Ali Ghavami, Dersy M. Lugo, Gudrun Lotze, Otto Virtanen, Peter Beumers, Jan Skov Pedersen, Andre Bardow, Roland G. Winkler, and Walter Richtering. Time-resolved structural evolution during the collapse of responsive hydrogels: The microgel-to-particle transition. *Science Advances*, 4(4):eaao7086, apr 2018. doi: 10.1126/sciadv.aao7086.

[57] J.-H. Kim and M. Ballauff. The volume transition in thermosensitive core-shell latex particles containing charged groups. *Colloid & Polymer Science*, 277(12):1210–1214, dec 1999. doi: 10.1007/s003960050512.

[58] Dennis E. Koppel. Analysis of macromolecular polydispersity in intensity correlation spectroscopy: The method of cumulants. *The Journal of Chemical Physics*, 57(11):4814–4820, 1972. ISSN 0021-9606.

[59] Elena Yu. Kozhunova, Vladimir Yu. Rudyak, Xiang Li, Mitsuhiro Shibayama, Georgy S. Peters, Oxana V. Vyshivannaya, Irina R. Nasimova, and Alexander V. Chertovich. Microphase separation of stimuli-responsive interpenetrating network microgels investigated by scattering

methods. *Journal of Colloid and Interface Science*, 597:297–305, sep 2021. doi: 10.1016/j.jcis.2021.03.178.

[60] Karl Kratz, Thomas Hellweg, and Wolfgang Eimer. Influence of charge density on the swelling of colloidal poly(*N*-isopropylacrylamide-co-acrylic acid) microgels. *Colloids and Surfaces A: Physicochemical and Engineering Aspects*, 170(2-3):137–149, sep 2000. doi: 10.1016/s0927-7757(00)00490-8.

[61] Karl Kratz, Thomas Hellweg, and Wolfgang Eimer. Structural changes in PNIPAM microgel particles as seen by SANS, DLS, and EM techniques. *Polymer*, 42(15):6631–6639, jul 2001. doi: 10.1016/s0032-3861(01)00099-4.

[62] Takuma Kureha, Yasuhisa Nagase, and Daisuke Suzuki. High reusability of catalytically active gold nanoparticles immobilized in core–shell hydrogel microspheres. *ACS Omega*, 3(6):6158–6165, jun 2018. doi: 10.1021/acsomega.8b00819.

[63] Tetyana Kyrey, Judith Witte, Artem Feoktystov, Vitaliy Pipich, Baohu Wu, Stefano Pasini, Aurel Radulescu, Marcus U. Witt, Margarita Kruteva, Regine von Klitzing, Stefan Wellert, and Olaf Holderer. Inner structure and dynamics of microgels with low and medium crosslinker content prepared via surfactant-free precipitation polymerization and continuous monomer feeding approach. *Soft Matter*, 15(32):6536–6546, 2019. doi: 10.1039/c9sm01161g.

[64] A. Kniger, N. Plack, W. Khler, M. Siebenbrger, and M. Ballauff. Thermophoresis of thermoresponsive polystyrene–poly(n-

isopropylacrylamide) core–shell particles. *Soft Matter*, 9(5):1418–1421, 2013. doi: 10.1039/c2sm27417e.

[65] Thomas Lane, Julianne L. Holloway, Amir H. Milani, Jennifer M. Saunders, Anthony J. Freemont, and Brian R. Saunders. Double network hydrogels prepared from pH-responsive doubly crosslinked microgels. *Soft Matter*, 9(33):7934, 2013. doi: 10.1039/c3sm51356d.

[66] Livie Lienafa, Julian Oberdisse, Serge Mora, Sophie Monge, and Jean-Jacques Robin. Rheology and SANS on PET-b-PLAc-b-p(DMAEMAq) triblock copolymers: Impact of the PET and polyelectrolyte chain length. *Macromolecules*, 44(13):5326–5335, jul 2011. doi: 10.1021/ma200331b.

[67] P. Lindner and Thomas Zemb, editors. *Neutrons, X-rays and light : scattering methods applied to soft condensed matter*. North-Holland, 2002. ISBN 978-0444511225.

[68] Simon Mallam, Ferenc Horkay, Anne Marie Hecht, and Erik Geissler. Scattering and swelling properties of inhomogeneous polyacrylamide gels. *Macromolecules*, 22(8):3356–3361, aug 1989. doi: 10.1021/ma00198a029.

[69] R. L. McGreevy and L. Pusztai. Reverse monte carlo simulation: A new technique for the determination of disordered structures. *Molecular Simulation*, 1(6):359–367, dec 1988. doi: 10.1080/08927028808080958.

[70] Yu Mei, Yan Lu, Frank Polzer, Matthias Ballauff, and Markus Drechsler. Catalytic activity of palladium nanoparticles encapsulated in spherical polyelectrolyte brushes and core-shell microgels. *Chemistry of Materials*, 19(5):1062–1069, mar 2007. doi: 10.1021/cm062554s.

[71] Norberto Micali, Monica Bertoldo, Elena Buratti, Valentina Nigro, Roberta Angelini, and Valentina Villari. Interpenetrating polymer network microgels in water: Effect of composition on the structural properties and electrosteric interactions. *ChemPhysChem*, 19(21):2894–2901, sep 2018. doi: 10.1002/cphc.201800707.

[72] Dafne Musino, Anne-Caroline Genix, Edouard Chauveau, Thomas Bizien, and Julian Oberdisse. Structural identification of percolation of nanoparticles. *Nanoscale*, 12(6):3907–3915, 2020. doi: 10.1039/c9nr09395h.

[73] Satish Nayak and L. Andrew Lyon. Soft nanotechnology with soft nanoparticles. *Angewandte Chemie*, 44(47):7686–7708, 2005. ISSN 0044-8249. doi: 10.1002/anie.200501321.

[74] Anne C. Nickel, Andrea Scotti, Judith E. Houston, Thiago Ito, Jérôme Crassous, Jan Skov Pedersen, and Walter Richtering. Anisotropic hollow microgels that can adapt their size, shape, and softness. *Nano Letters*, 19(11):8161–8170, oct 2019. doi: 10.1021/acs.nanolett.9b03507.

[75] V. Nigro, R. Angelini, S. King, S. Franco, E. Buratti, F. Bomboi, N. Mahmoudi, F. Corvasce, R. Scaccia, A. Church, T. Charleston, and B. Ruzicka. Apparatus for simultaneous dynamic light scattering–small angle neutron scattering investigations of dynamics and structure in soft matter. *Review of Scientific Instruments*, 92(2):023907, feb 2021. doi: 10.1063/5.0035529.

[76] Sofi Nöjd, Peter Holmqvist, Niels Boon, Marc Obiols-Rabasa, Priti S. Mohanty, Ralf Schweins, and Peter Schurtenberger. Deswelling behaviour

of ionic microgel particles from low to ultra-high densities. *Soft Matter*, 14(20):4150–4159, 2018. doi: 10.1039/c8sm00390d.

[77] Sofi Njd, Christopher Hirst, Marc Obiols-Rabasa, Julien Schmitt, Aurel Radulescu, Priti S. Mohanty, and Peter Schurtenberger. Soft particles in an electric field – a zero average contrast study. *Soft Matter*, 15(31): 6369–6374, 2019. doi: 10.1039/c9sm01208g.

[78] Julian Oberdisse and Bruno Demé. Structure of latex-silica nanocomposite films: a small-angle neutron scattering study. *Macromolecules*, 35 (11):4397–4405, apr 2002. doi: 10.1021/ma0118419.

[79] Julian Oberdisse, Peter Hine, and Wim Pyckhout-Hintzen. Structure of interacting aggregates of silicananoparticles in a polymer matrix: small-angle scattering and reverse monte carlo simulations. *Soft Matter*, 3(4): 476–485, 2007. doi: 10.1039/b614957j.

[80] R. H. Pelton and P. Chibante. Preparation of aqueous latices with N-isopropylacrylamide. *Colloids and Surfaces*, 20(3):247–256, 1986. ISSN 01666622. doi: 10.1016/0166-6622(86)80274-8.

[81] Robert Pelton. Temperature-sensitive aqueous microgels. *Advances in Colloid and Interface Science*, 85(1):1–33, feb 2000. doi: 10.1016/s0001-8686(99)00023-8.

[82] Dmitry V. Pergushov, Larisa V. Sigolaeva, Nadezhda G. Balabushevich, Timur Z. Sharifullin, Michael Noyong, and Walter Richtering. Loading of doxorubicin into surface-attached stimuli-responsive microgels and its subsequent release under different conditions. *Polymer*, 213:123227, jan 2021. doi: 10.1016/j.polymer.2020.123227.

[83] Andrij Pich and Walter Richtering. Microgels by precipitation polymerization: Synthesis, characterization, and functionalization. In *Chemical Design of Responsive Microgels*, pages 1–37. Springer Berlin Heidelberg, 2010. doi: 10.1007/12_2010_70.

[84] Felix A. Plamper and Walter Richtering. Functional microgels and microgel systems. *Accounts of Chemical Research*, 50(2):131–140, feb 2017. doi: 10.1021/acs.accounts.6b00544.

[85] Stephen W. Provencher. CONTIN: A general purpose constrained regularization program for inverting noisy linear algebraic and integral equations. *Computer Physics Communications*, 27(3):229–242, sep 1982. doi: 10.1016/0010-4655(82)90174-6.

[86] Chantal Rufier, André Collet, Michel Viguier, Julian Oberdisse, and Serge Mora. Influence of surfactants on hydrophobically end-capped poly(ethylene oxide) self-assembled aggregates studied by SANS. *Macromolecules*, 44(18):7451–7459, sep 2011. doi: 10.1021/ma201150g.

[87] Brian R. Saunders. On the structure of poly(n-isopropylacrylamide) microgel particles. *Langmuir*, 20(10):3925–3932, may 2004. doi: 10.1021/la036390v.

[88] Brian R. Saunders and Brian Vincent. Microgel particles as model colloids: theory, properties and applications. *Advances in Colloid and Interface Science*, 80(1):1–25, feb 1999. doi: 10.1016/s0001-8686(98)00071-2.

[89] Brian R. Saunders, Helen M. Crowther, and Brian Vincent. Poly[(methyl methacrylate)-co-(methacrylic acid)] microgel particles: swelling control

using pH, cononsolvency, and osmotic deswelling. *Macromolecules*, 30 (3):482–487, feb 1997. doi: 10.1021/ma961277f.

[90] Wolfgang Schärtl. *Light Scattering from Polymer Solutions and Nanoparticle Dispersions*. Springer Berlin Heidelberg, 2007. doi: 10.1007/978-3-540-71951-9.

[91] C. Scherzinger, O. Holderer, D. Richter, and W. Richtering. Polymer dynamics in responsive microgels: influence of cononsolvency and microgel architecture. *Physical Chemistry Chemical Physics*, 14(8):2762, 2012. doi: 10.1039/c2cp23328b.

[92] D. Schmaljohann. Thermo- and pH-responsive polymers in drug delivery. *Advanced Drug Delivery Reviews*, 58(15):1655–1670, dec 2006. doi: 10.1016/j.addr.2006.09.020.

[93] Andreas J. Schmid, Janine Dubbert, Andrey A. Rudov, Jan Skov Pedersen, Peter Lindner, Matthias Karg, Igor I. Potemkin, and Walter Richtering. Multi-shell hollow nanogels with responsive shell permeability. *Scientific Reports*, 6(1), mar 2016. doi: 10.1038/srep22736.

[94] Andreas Josef Schmid, Lars Wiehemeier, Sebastian Jaksch, Harald Schneider, Arno Hiess, Torsten Bögershausen, Tobias Widmann, Julija Reitenbach, Lucas P. Kreuzer, Matthias Kühnhammer, Oliver Löhmann, Georg Brandl, Henrich Frielinghaus, Peter Müller-Buschbaum, Regine von Klitzing, and Thomas Hellweg. Flexible sample environments for the investigation of soft matter at the european spallation source: Part I —the in situ SANS/DLS setup. *Applied Sciences*, 11(9):4089, apr 2021. doi: 10.3390/app11094089.

[95] Florian Schneider, Andreea Balaceanu, Zhenyu Di, Yuri B. Melnichenko, Jürgen Allgaier, Andrij Pich, Gerald J. Schneider, and Dieter Richter. Internal structure and phase transition behavior of stimuli-responsive microgels in PEG melts. *Soft Matter*, 13(15):2738–2748, 2017. doi: 10.1039/c6sm02501c.

[96] Jochen Schneider, Malte Wiemann, Anna Rabe, and Eckhard Bartsch. On tuning microgel character and softness of cross-linked polystyrene particles. *Soft Matter*, 13(2):445–457, 2017. doi: 10.1039/c6sm02007k.

[97] A. Scotti, W. Liu, J. S. Hyatt, E. S. Herman, H. S. Choi, J. W. Kim, L. A. Lyon, U. Gasser, and A. Fernandez-Nieves. The CONTIN algorithm and its application to determine the size distribution of microgel suspensions. *The Journal of Chemical Physics*, 142(23):234905, jun 2015. doi: 10.1063/1.4921686.

[98] A. Scotti, U. Gasser, E. S. Herman, Jun Han, A. Menzel, L. A. Lyon, and A. Fernandez-Nieves. Phase behavior of binary and polydisperse suspensions of compressible microgels controlled by selective particle deswelling. *Physical Review E*, 96(3), sep 2017. doi: 10.1103/physreve.96.032609.

[99] A. Scotti, M. Brugnoni, A. A. Rudov, J. E. Houston, I. I. Potemkin, and W. Richtering. Hollow microgels squeezed in overcrowded environments. *The Journal of Chemical Physics*, 148(17):174903, may 2018. doi: 10.1063/1.5026100.

[100] A. Scotti, J. E. Houston, M. Brugnoni, M. M. Schmidt, M. F. Schulte, S. Bochenek, R. Schweins, A. Feoktystov, A. Radulescu, and W. Richtering. Phase behavior of ultrasoft spheres show stable bcc lattices. *Physical Review E*, 102(5), nov 2020. doi: 10.1103/physreve.102.052602.

[101] Andrea Scotti. Characterization of the volume fraction of soft deformable microgels by means of small-angle neutron scattering with contrast variation. *Soft Matter*, 17(22):5548–5559, 2021. doi: 10.1039/d1sm00277e.

[102] Andrea Scotti, Urs Gasser, Emily S. Herman, Miguel Pelaez-Fernandez, Jun Han, Andreas Menzel, L. Andrew Lyon, and Alberto Fernández-Nieves. The role of ions in the self-healing behavior of soft particle suspensions. *Proceedings of the National Academy of Sciences*, 113(20): 5576–5581, apr 2016. doi: 10.1073/pnas.1516011113.

[103] Andrea Scotti, Alan R. Denton, Monia Brugnoni, Judith E. Houston, Ralf Schweins, Igor I. Potemkin, and Walter Richtering. Deswelling of microgels in crowded suspensions depends on cross-link density and architecture. *Macromolecules*, 52(11):3995–4007, may 2019. doi: 10.1021/acs.macromol.9b00729.

[104] S. Seelenmeyer, I. Deike, N. Dingenouts, S. Rosenfeldt, Ch. Norhausen, M. Ballauff, and T. Narayanan. Analysis of the volume transition in thermosensitive core-shell particles by synchrotron small-angle x-ray scattering. *Journal of Applied Crystallography*, 33(3):574–576, jun 2000. doi: 10.1107/s0021889899013163.

[105] S. Seelenmeyer, I. Deike, S. Rosenfeldt, Ch. Norhausen, N. Dingenouts, M. Ballauff, T. Narayanan, and P. Lindner. Small-angle x-ray and neutron scattering studies of the volume phase transition in thermosensitive core–shell colloids. *The Journal of Chemical Physics*, 114(23):10471–10478, jun 2001. doi: 10.1063/1.1374633.

[106] Michael J. Serpe, Kristen A. Yarmey, Christine M. Nolan, and L. An-

drew Lyon. Doxorubicin uptake and release from microgel thin films. *Biomacromolecules*, 6(1):408–413, jan 2005. doi: 10.1021/bm049455x.

[107] Mitsuhiro Shibayama, Toyoichi Tanaka, and Charles C. Han. Small angle neutron scattering study on poly(N-isopropyl acrylamide) gels near their volume-phase transition temperature. *The Journal of Chemical Physics*, 97(9):6829–6841, nov 1992. doi: 10.1063/1.463636.

[108] Tong Shu, Qiming Shen, Yu Wan, Wei Zhang, Lei Su, Xueji Zhang, and Michael J. Serpe. Silver nanoparticle-loaded microgel-based etalons for h2o2sensing. *RSC Advances*, 8(28):15567–15574, 2018. doi: 10.1039/c8ra02215a.

[109] Martin J. Snowden, Babur Z. Chowdhry, Brian Vincent, and Gayle E. Morris. Colloidal copolymer microgels of N-isopropylacrylamide and acrylic acid: pH, ionic strength and temperature effects. *Journal of the Chemical Society, Faraday Transactions*, 92(24):5013, 1996. doi: 10.1039/ft9969205013.

[110] Markus Stieger, Walter Richtering, Jan Skov Pedersen, and Peter Lindner. Small-angle neutron scattering study of structural changes in temperature sensitive microgel colloids. *The Journal of Chemical Physics*, 120(13):6197–6206, apr 2004. doi: 10.1063/1.1665752.

[111] Toyoichi Tanaka and David J. Fillmore. Kinetics of swelling of gels. *The Journal of Chemical Physics*, 70(3):1214–1218, feb 1979. doi: 10.1063/1.437602.

[112] J. Teixeira. Small-angle scattering by fractal systems. *Journal*

of Applied Crystallography, 21(6):781–785, dec 1988. doi: 10.1107/s0021889888000263.

[113] Rodica Turcu, Izabell Craciunescu, Vasil M. Garamus, Christina Janko, Stefan Lyer, Rainer Tietze, Christoph Alexiou, and Ladislau Vekas. Magnetic microgels for drug targeting applications: Physical–chemical properties and cytotoxicity evaluation. *Journal of Magnetism and Magnetic Materials*, 380:307–314, apr 2015. doi: 10.1016/j.jmmm.2014.08.041.

[114] Katja Uhlig, Thomas Wegener, Yvonne Hertle, Johannes Bookhold, Magnus Jaeger, Thomas Hellweg, Andreas Fery, and Claus Duschl. Thermoresponsive microgel coatings as versatile functional compounds for novel cell manipulation tools. *Polymers*, 10(6):656, jun 2018. doi: 10.3390/polym10060656.

[115] O. L. J. Virtanen, A. Mourran, P. T. Pinard, and W. Richtering. Persulfate initiated ultra-low cross-linked poly(*N*-isopropylacrylamide) microgels possess an unusual inverted cross-linking structure. *Soft Matter*, 12(17):3919–3928, 2016. doi: 10.1039/c6sm00140h.

[116] Otto L. J. Virtanen, Michael Kather, Julian Meyer-Kirschner, Andrea Melle, Aurel Radulescu, Jörn Viell, Alexander Mitsos, Andrij Pich, and Walter Richtering. Direct monitoring of microgel formation during precipitation polymerization of *N*-isopropylacrylamide using in situ SANS. *ACS Omega*, 4(2):3690–3699, feb 2019. doi: 10.1021/acsomega.8b03461.

[117] Menglian Wei and Michael J. Serpe. Temperature-light dual-responsive Au@PNIPAm core-shell microgel-based optical devices. *Particle & Particle Systems Characterization*, 36(1):1800326, nov 2018. doi: 10.1002/ppsc.201800326.

[118] Nicole Welsch, Matthias Ballauff, and Yan Lu. Microgels as nanoreactors: Applications in catalysis. In *Chemical Design of Responsive Microgels*, pages 129–163. Springer Berlin Heidelberg, 2010. doi: 10.1007/12_2010_71.

[119] Tobias Widmann, Lucas P. Kreuzer, Nuri Hohn, Lorenz Bießmann, Kun Wang, Stephan Rinner, Jean-François Moulin, Andreas J. Schmid, Yvonne Hannappel, Oliver Wrede, Matthias Kühnhammer, Thomas Hellweg, Regine von Klitzing, and Peter Müller-Buschbaum. Hydration and solvent exchange induced swelling and deswelling of homogeneous poly(*N*-isopropylacrylamide) microgel thin films. *Langmuir*, 35(49): 16341–16352, nov 2019. doi: 10.1021/acs.langmuir.9b03104.

[120] Oliver Wrede, Yvonne Reimann, Stefan Lülsdorf, Daniel Emmrich, Kristina Schneider, Andreas Josef Schmid, Diana Zauser, Yvonne Hannappel, André Beyer, Ralf Schweins, Armin Gölzhäuser, Thomas Hellweg, and Thomas Sottmann. Volume phase transition kinetics of smart *N*-*n*-propylacrylamide microgels studied by time-resolved pressure jump small angle neutron scattering. *Scientific Reports*, 8(1), sep 2018. doi: 10.1038/s41598-018-31976-4.

[121] Qingwen Wu, Chao Lv, Zhijun Zhang, Yuqing Li, Jingjing Nie, Junting Xu, and Binyang Du. Poly(*N*-isopropylacrylamide-co-1-vinyl-3-alkylimidazolium bromide) microgels with internal nanophase-separated structures. *Langmuir*, 34(31):9203–9214, jul 2018. doi: 10.1021/acs.langmuir.8b01575.

[122] Sarah K. Wypysek, Andrea Scotti, Mohammed O. Alziyadi, Igor I. Potemkin, Alan R. Denton, and Walter Richtering. Tailoring the cavity

of hollow polyelectrolyte microgels. *Macromolecular Rapid Communications*, 41(1):1900422, nov 2019. doi: 10.1002/marc.201900422.

[123] Michael Zeiser, Ines Freudensprung, and Thomas Hellweg. Linearly thermoresponsive core–shell microgels: Towards a new class of nanoactuators. *Polymer*, 53(26):6096–6101, dec 2012. doi: 10.1016/j.polymer.2012.10.001.